Quantitative Control over Electrodeposition of Silica Films onto Single-Walled Carbon Nanotube Surfaces†

Mandakini Kanungo,‡ Hugh S. Isaacs,‡ and Stanislaus S. Wong*,‡,§

Condensed Matter Physics and Materials Sciences Department, Brookhaven National Laboratory, Building 480, Upton, New York 11973, and Department of Chemistry, State University of New York at Stony Brook, Stony Brook, New York 11794-3400

Received: December 27, 2006; In Final Form: February 4, 2007

Control over the thickness of a silica coating on single-walled carbon nanotubes (SWNTs) is highly desirable for applications in optics and in biomedicine. Moreover, a silica coating on SWNTs would also aid in avoiding tube−tube contact and bundle formation as well as tube oxidation, a scenario conducive to the use of appropriately functionalized carbon nanotubes as individualized gate dielectric materials in field effect transistors. In this work, we have developed two feasible and reliable means with which to coat SWNTs with various reproducible thicknesses of silica using an electrochemical sol−gel process. In one procedure, a SWNT mat was used as a working electrode for the direct deposition of silica. In the second, nanotubes were dispersed in solution and silica was deposited onto these solubilized nanotubes in the presence of a platinum working electrode. Applying a negative potential results in the condensation of a silica film onto the SWNT surface. The thickness of the silica coating can be controllably altered by varying the potential of the working electrode as well as the concentration of the sol solution. These methodologies have the advantages of ease of use, environmental friendliness, and utilization of relatively mild reaction conditions.

Introduction

The remarkable structure-dependent optical, electronic, and mechanical properties of single-walled carbon nanotubes (SWNTs)[1] have attracted a lot of attention over the past decade due to their potential in applications as varied as molecular electronics, sensing, gas storage, field emission applications, catalyst supports, probes for scanning probe microscopy, and components in high-performance composites.[2−4] Chemical functionalization[5−8] has been used as a route toward rationally tailoring the properties of carbon nanotubes so they can be incorporated into functional devices and architectures. One of the particularly promising and as yet relatively unexplored areas of research involves coating of SWNTs with insulating materials to fabricate nanotube-based devices such as field effect transistors (FETs), single-electron transistors, and gas sensors.[9−11]

In general, the synthesis of a carbon nanotube−insulator heterostructure is important for the use of carbon nanotubes in applications ranging from FET devices to molecular circuits and switches. Specifically, carbon nanotube−silica heterostructure composites are particularly intriguing because of the well-known insulating properties of silica. Indeed, carbon nanotube−silica composites are often critical for applications ranging from electronics and optics to biology. A protective coating of silica can limit the perturbation of the desirable mechanical and electronic properties of nanotubes, while simultaneously providing for a means to functionalize these nanoscale species. In addition, a thin SiO_2/SiO_x coating is optically transparent, and moreover, silica is well-known for its biomolecular compatibility. Furthermore, it is envisaged that the coating of thin, transparent silica on carbon nanotube surfaces would enable their utilization in applications associated with biomedical optics.

Two general strategies have been utilized for silica functionalization of carbon nanotubes. One involves covalent functionalization of silica onto carbon nanotube sidewalls using a range of either silyl or silane derivatives.[12−16] Though covalent functionalization is a robust and a well-controlled process, it may also seriously compromise or otherwise destroy the desirable electronic and optical properties of the carbon nanotubes to a large extent. An alternative strategy has been to coat carbon nanotubes with silica using a noncovalent methodology. A recent theoretical study has shown that a nonbonded, protective layer of silica only weakly perturbs the electronic structure of single walled carbon nanotubes (SWNTs).[17] Therefore, for optimal performance, the existence of a protective layer of silica on the carbon nanotubes should not only enable the retention of desirable electronic, mechanical, and optical properties of carbon nanotubes but also simultaneously and nondestructively functionalize these nanoscale species for a number of diverse applications.

Experimentally, multiwalled carbon nanotubes (MWNTs) coated with silica at room-temperature reveal a higher oxidation resistance and better mechanical properties when compared with heavily processed tubes.[18] An increase in thermal conductivity has been reported for homogeneous MWNT−SiO_2 composites,[19] whereas MWNT/silica xerogel composites have been shown to display enhanced nonlinear optical properties, relative to those of underivatized MWNTs.[20] In addition, MWNT−sol gel composite materials, depending on the nature of the silane precursors used in their fabrication, have been reported to show faster electron-transfer rates and a wide range of favorable capacitance values, thereby providing for enhanced capabilities in the development of novel electrochemical devices using these composites.[21] However, control over the thickness of such a

† Part of the special issue "Richard E. Smalley Memorial Issue".

* To whom correspondence should be addressed. Phone: 631-632-1703; 631-344-3178. E-mail: sswong@notes.cc.sunysb.edu; sswong@bnl.gov.

‡ Brookhaven National Laboratory.

§ State University of New York at Stony Brook.

10.1021/jp068967y CCC: $37.00
Published on Web 04/20/2007

AFM height images of silica-coated nanotubes synthesized by electrochemical deposition of carbon nanotubes dispersed in the solution. (iv) Additional HRTEM images of nanotubes electrodeposited with Si. (v) SEM image and corresponding EDS spectrum of a control sample. (vi) High-resolution XPS spectra of purified single-walled carbon nanotubes. (vii) High-resolution XPS spectra of a control sample. (viii) High-resolution XPS spectra of silica-coated nanotubes. This material is available free of charge via the Internet at http://pubs.acs.org.

References and Notes

(1) Iijima, S. *Nature* **1991**, *354*, 56.

(2) Dresselhaus, M. S.; Dresselhaus, G.; Avouris, P. *Carbon Nanotubes: Synthesis, Structure, Properties, and Applications*; Springer-Verlag: Berlin, 2001.

(3) Baughman, R. H.; Zakhidov, A. A.; de Heer, W. A. *Science* **2002**, *297*, 787.

(4) Avouris, P. *Acc. Chem. Res.* **2002**, *35*, 1026.

(5) Bahr, J.; Tour, J. M. *J. Mater. Chem.* **2002**, *12*, 1952.

(6) Hirsch, A. *Angew. Chem., Int. Ed* **2002**, *41*, 1853.

(7) Chen, J.; Hamon, M. A.; Hu, H.; Chen, Y.; Rao, A. M.; Eklund, P. C.; Haddon, R. C. *Science* **1998**, *282*, 95.

(8) Banerjee, S.; Hemraj-Benny, T.; Wong, S. S. *Adv. Mater.* **2005**, *17*, 17.

(9) Wind, S.; Appenzeller, J.; Martel, R.; Derycke, V.; Avouris, P. *Appl. Phys. Lett.* **2002**, *80*, 3817.

(10) Postma, H. W. C.; Teepen, T.; Yao, Z.; Grifoni, M.; Dekker, C. *Science* **2001**, *293*, 76.

(11) Kong, J.; Franklin, N. R.; Zhou, C.; Chapline, M. G.; Peng, S.; Cho, K.; Dai, H. *Science* **2000**, *287*, 622.

(12) Bottini, M.; Tautz, L.; Huynh, H.; Monosov, E.; Bottini, N.; Dawson, M. I.; Bellucci, S.; Mustelin, T. *Chem. Commun.* **2005**, *6*, 758.

(13) Vast, L.; Philippin, G.; Destree, A.; Moreau, N.; Fonseca, A.; Nagy, J. B.; Delhalle, J.; Mekhalif, Z. *Nanotechnology* **2004**, *15*, 781.

(14) Velasco- Santos, C.; Martinez-Hernadez, A. L.; Lozada-Cassou, M.; Alvarez-Castillo, A.; Castano, V. M. *Nanotechnology* **2002**, *13*, 495.

(15) Aizawa, M.; Shaffer, M. S. P. *Chem. Phys. Lett.* **2003**, *368*, 121.

(16) Fan, W.; Gao, L. *Chem. Lett.* **2005**, *34*, 954.

(17) Wojdel, J. C.; Bromley, S. T. *J. Phys. Chem. B* **2005**, *109*, 1387.

(18) Seeger, T.; Köhler, T.; Frauenheim, T.; Grobert, N.; Rühle, M.; Terrones, M.; Seifert, G. *Chem. Commun.* **2002**, *1*, 34.

(19) Ning, J.; Zhang, J.; Pan, Y.; Guo, J. *J. Mater. Sci. Lett.* **2003**, *22*, 1019.

(20) Hongbing, Z.; Chan, Z.; Wenzhe, C.; Minquan, W. *Chem. Phys. Lett.* **2005**, *411*, 373.

(21) Gavalas, V. G.; Andrews, R.; Bhattacharyya, D.; Bachas, L. G. *Nano Lett.* **2001**, *1*, 719.

(22) Coradin, T.; Lopez, P. J. *ChemBioChem* **2003**, *4*, 251.

(23) Ikuno, T.; Katayama, M.; Kamada, K.; Honda, S.-i.; Lee, J.-G.; Mori, H.; Oura, K. *Jpn. J. Appl. Phys.* **2003**, *42*, L1356.

(24) Ikuno, T.; Katyama, M.; Lee, K.-Y.; Kuzuoka, T.; Lee, J-G.; Honda, S.-i.; Mori, H.; Oura, K. *Jpn. J. Appl. Phys.* **2004**, *43*, L987.

(25) Fu, Q.; Lu, C.; Liu, J. *Nano Lett.* **2002**, *2*, 329.

(26) Whitsitt, E. A.; Barron, A. R. *Nano Lett.* **2003**, *3*, 775.

(27) Whitsitt, E. A.; Moore, V. C.; Smalley, R. E.; Barron, A. R. *J. Mater. Chem.* **2005**, *15*, 4678.

(28) Colorado, R. J.; Barron, A. R. *J. Mater. Chem.* **2004**, *16*, 2692.

(29) Colorado, R. J.; Diosomito, M. E.; Barron, A. R. *Adv. Mater.* **2005**, *17*, 1634.

(30) Pender, M. J.; Sowards, L. S.; Hartgerink, J. D.; Stone, M. O.; Naik, R. J. *Nano Lett.* **2006**, *6*, 40.

(31) Berguiga, L.; Bellessa, J.; Vocanson, F.; Bernstein, E.; Plenet, J. C. *Opt. Mater.* **2006**, *28*, 167.

(32) Liu, Y.; Tang, J.; Chen, X.; Wang, R.; Pang, G. K. H.; Zhang, Y.; Xin, J. H. *Carbon* **2006**, *44*, 158.

(33) Seeger, T.; Redlich, P.; Grobert, N.; Terrones, M.; Walton, D. R. M.; Kroto, H. W.; Rühle, M. *Chem. Phys. Lett.* **2001**, *339*, 41.

(34) Chiang, I. W.; Brinson, B. E.; Huang, A. Y.; Willis, P. A.; Bronikowski, M. J.; Margrave, J. L.; Smalley, R. E.; Hauge, R. H. *J. Phys. Chem. B* **2001**, *105*, 8297.

(35) Park, T.-J.; Banerjee, S.; Hemraj-Benny, T.; Wong, S. S. *J. Mater. Chem.* **2006**, *16*, 141.

(36) Deepa, P. N.; Kanungo, M.; Claycomb, G.; Sherwood, P. M. A.; Collinson, M. M. *Anal. Chem.* **2003**, *75*, 5399.

(37) Shacham, R.; Anvir, D.; Mandler, D. *Adv. Mater.* **1999**, *11*, 384.

(38) Bard, A. J.; Faulkner, I. R. *Electrochemical Methods. Fundamentals and Applications*; Wiley: New York, 1980.

(39) Bockris, J. O. M.; Khan, S. U. M. *Surface Electrochemistry*; Plenum: New York, 1993.

(40) Aldykiewicz, A. J., Jr.; Davenport, A. J.; Isaacs, H. S. *J. Electrochem. Soc.* **1996**, *143*, 147.

(41) Kuhn, A. T.; Chan, C. Y. *J. Appl. Electrochem.* **1983**, *13*, 189.

(42) Li, J.-L.; Kudin, K.; McAllister, M. J.; Prudhomme, R. K.; Aksay, I. A.; Car, R. *Phys. Rev. Lett.* **2006**, *96*, 176101.

(43) Iler, R. K. *The Chemistry of Silica*; Wiley: New York, 1979.

(44) Brinker, C. J.; Frye, G. C.; Hurd, A. J.; Ashley, C. S. *Thin Solid Films* **1991**, *201*, 97.

(45) Okpalugo, T. I. T.; Papakonstantinou, P.; Murphy, H.; McLaughlin, J.; Brown, N. M. D. *Carbon* **2005**, *43*, 153.

(46) Martinez, M. T.; Callejas, M. A.; Benito, A. M.; Cochet, M.; Seeger, T.; Anson, A.; Schreiber, J.; Gordon, C.; Marhic, C.; Chauvet, O.; Fierro, J. L. G.; Maser, W. K. *Carbon* **2003**, *41*, 2247.

(47) Bahr, J. L.; Tour, J. M. *Chem. Mater.* **2001**, *13*, 3823.

(48) Tour, J. M.; Dyke, C. A. *Chem. Eur. J.* **2004**, *10*, 812.

(49) Sen, R.; Rickard, S. M.; Itkis, M. E.; Haddon, R. C. *Chem. Mater.* **2003**, *15*, 4723.

(50) Krupke, R.; Hennrich, F.; Hampe, O.; Kappes, M. M. *J. Phys. Chem. B* **2003**, *107*, 5667.

(51) Huang, H.; Kajiura, H.; Maruyama, R.; Kadono, K.; Noda, K. *J. Phys. Chem. B* **2006**, *110*, 4686.

(52) Banerjee, S.; Wong, S. S. *J. Am. Chem. Soc.* **2004**, *126*, 2073.

(53) Dresselhaus, M. S.; Dresselhaus, G.; Saito, R. *Phys. Rep.* **2005**, *409*, 47.

(54) Dresselhaus, M. S.; Dresselhuas, G.; Jorio, A.; Souza Filho, A. G.; Pimenta, M. A.; Saito, R. *Acc. Chem. Res.* **2002**, *35*, 1070.

(55) Rao, A. M.; Richter, E.; Bandow, S.; Chase, B.; Eklund, P. C.; Williams, K. A.; Fang, S.; Subbaswamy, K. R.; Menon, M.; Thess, A.; Smalley, R. E.; Dresselhaus, G.; Dresselhaus, M. S. *Science* **1997**, *275*, 187.

(56) Yu, Z.; Brus, L. E. *J. Phys. Chem. B* **2001**, *105*, 1123.

(57) Brown, S. D. M.; Corio, P.; Marucci, A.; Pimenta, M. A.; Dresselhaus, M. S.; Dresselhaus, G. *Phys. Rev. B* **2000**, *61*, 7734.

(58) Chen, Z.; Ziegler, K. J.; Shaver, J.; Hauge, R. H.; Smalley, R. E. *J. Phys. Chem. B* **2006**, *110*, 11624.

(59) Dyke, C. A.; Tour, J. M. *J. Am. Chem. Soc.* **2003**, *125*, 1156.

(60) Osswald, S.; Flahaut, E.; Gogotsi, Y. *Chem. Mater.* **2006**, *18*, 1525.

(61) Bachilo, S. M.; Strano, M. S.; Kittrell, C.; Hauge, R. H.; Smalley, R. E.; Weisman, R. B. *Science* **2002**, *298*, 2361.

(62) Strano, M. S.; Doorn, S. K.; Haroz, E. H.; Kittrell, C.; Hauge, R. H.; Smalley, R. E. *Nano. Lett.* **2003**, *3*, 1091.

(63) Heller, D. A.; Barone, P. W.; Swanson, J. P.; Mayrhofer, R. M.; Strano, M. S. *J. Phys. Chem. B* **2004**, *108*, 6905.

(64) Karajanagi, S. S.; Yang, H.; Asuri, P.; Sellitto, E.; Dordick, J.; Kane, R. S. *Langmuir* **2006**, *22*, 1392.

(65) Hennrich, F.; Krupke, R.; Lebedkin, S.; Arnold, K.; Fischer, R.; Resasco, D. E.; Kappes, M. *J. Phys. Chem. B* **2005**, *109*, 10567.

(66) Strano, M. *J. Am. Chem. Soc.* **2003**, *125*, 16148.

(67) Krupke, R.; Hennrich, F.; Loehneysen, H. V.; Kappes, M. *Science* **2003**, *301*, 344.

(68) Chattopadhyay, D.; Galeska, I.; Papadimitrikopoulos, F. *J. Am. Chem. Soc.* **2003**, *125*, 3370.

(69) Strano, M. S.; Dyke, C. A.; Usrey, M. L.; Barone, P. W.; Allen, M. J.; Shan, H.; Kittrell, C.; Hauge, R. H.; Tour, J. M.; Smalley, R. E. *Science* **2003**, *301*, 1519.

(70) Banerjee, S.; Wong, S. S. *J. Phys. Chem. B* **2002**, *106*, 12144.

(71) Banerjee, S.; Wong, S. S. *Nano Lett.* **2004**, *4*, 1445.

Carbon nanotube guided formation of silicon oxide nanotrenches

HYE RYUNG BYON AND HEE CHEUL CHOI*

Department of Chemistry, Pohang University of Science and Technology (POSTECH), San 31, Hyoja-Dong, Nam-Gu, Pohang, Korea 790-784
*e-mail: choihc@postech.edu

Published online: 18 February 2007; doi:10.1038/nnano.2007.26

The potential applications of carbon nanotubes are varied[1–6]. Although it has long been known that solid carbon can reduce SiO_2 to its gaseous state at high temperatures[7], exploiting this reaction to pattern surfaces with carbon nanotubes has never been demonstrated. Here we show that carbon nanotubes can act as the carbon source to reduce (etch) silicon dioxide surfaces. By introducing small amounts of oxygen gas during the growth of single-walled carbon nanotubes (SWNTs) in the chemical vapour deposition (CVD) process, the nanotubes selectively etch one-dimensional nanotrenches in the SiO_2. The shape, length and trajectory of the nanotrenches are fully guided by the SWNTs. These nanotrenches can also serve as a mask in the fabrication of sub-10-nm metal nanowires. Combined with alignment techniques, well-ordered nanotrenches can be made for various high-density electronic components in the nanoelectronics industry.

In contrast to the web-like carbon nanotubes that are typically obtained by the CVD process in the absence of oxygen[8] (Fig. 1a), oxygen-assisted CVD has reproducibly produced SiO_2 nanotrenches with well-defined line shape, regardless of the doping types of the Si substrates (Fig. 1b, c). Several representative features of the nanotrenches, such as their shape, length and trajectory, provide a straightforward indication that carbon nanotubes are directly involved in the formation of the nanotrenches. The lengths of the nanotrenches extend to tens of micrometres and are only limited by the original lengths of the carbon nanotubes. The average width of the nanotrenches, measured at the full width-at-half maximum (FWHM) points from high-resolution transmission electron microscopy (HRTEM) cross-sectional images, is determined to be $\sim 9.8 \pm 2.4$ nm (13 images were examined) (Fig. 3f). It should be noted that atomic force microscopy (AFM) does not provide accurate width information owing to the finite size of the tip[9]. The HRTEM cross-sectional image also shows that the reaction proceeds anisotropically, resulting in wider top openings and narrower bottoms to the nanotrenches.

The main driving force for nanotrench formation is carbothermal reduction of SiO_2, where carbon nanotubes play the role of bulk carbon, C(s). Amorphous bulk silica, SiO_2(s), is known to be reduced by carbon at temperatures over 1,754 °C and under atmospheric pressure by releasing SiO(g) and CO(g), as shown in equation (1) (ref. 7).

$$SiO_2(s) + C(s) \rightleftharpoons SiO(g) + CO(g) \qquad (1)$$

Because both the solid-phase SiO_2 and C should be in contact with one another to enable the carbothermal reduction to occur, only the carbon nanotubes that make direct contact with the SiO_2 surface are active for the reaction (Fig. 2a). Indeed, most of the suspended carbon nanotubes are simply burned out during the process, which explains the population difference between the original carbon nanotubes and the nanotrenches (Fig. 1a and b). Incomplete reaction between the carbon nanotubes and the SiO_2 left some portions of the carbon nanotubes unreacted at the ends of the nanotrenches, further confirming the role of carbon nanotubes in guiding the formation of the nanotrenches (Fig. 2b, c). According to equation (1), the formation of nanotrenches should be highly selective to the SiO_2 series of substrates, and we have found that nanotrenches are efficiently formed on quartz, but not on Si_3N_4 substrates (see Supplementary Information, Fig. S1).

Including small amounts of oxygen is key to triggering the destruction of carbon nanotubes[10,11], generating locally confined reactive carbonaceous species that readily react with the SiO_2 below at the same temperature. The efficiency of nanotrench formation is directly affected by the levels of oxygen and hydrocarbon gases. No nanotrench has been formed with an oxygen concentration lower than ~0.01% of total gases, but a much higher yield of nanotrenches has been obtained with 0.1% of added oxygen; above these oxygen levels no reaction has been attempted because of safety issues. Similarly, co-supplied hydrocarbon gases also accelerate the reduction of the SiO_2 surface. When the average volume of the nanotrenches formed and the stoichiometric reaction between SiO_2 and C are considered, the amount of carbon provided just by the carbon nanotubes (average diameter = 1.7 nm) is seen to be insufficient to etch out the entire underlying SiO_2 layer to form the nanotrenches. Hence, additional etching of SiO_2 seems to occur by means of externally supplied fragmentized hydrocarbons.

Iron catalyst nanoparticles also play an important role in the efficient carbothermal reduction of SiO_2. No nanotrench is formed when cobalt catalyst nanoparticles are used, although the nanoparticles still act as a catalyst to enable the growth of SWNTs (Fig. 2d). Iron nanoparticles are known to accelerate the thermal evaporation of SiO_2(s) into its gaseous state under low oxygen partial pressure[12,13]. Carbothermal reduction of SiO_2 is initiated from the spots where iron nanoparticles wrapped with carbon nanotubes are in contact with the SiO_2. Once the iron nanoparticles initiate the SiO_2 reduction, self-propagating carbothermal reduction creates further nanotrenches, and the nanoparticles are removed by evaporation or by the steady flow of gases over the surface. Indeed, most of the nanotrenches do not contain iron nanoparticles on either of their ends (Fig. 2f). Evidence for the removal of the iron nanoparticles is also

AES data were collected. The electron primary beam energy was 25 kV, and the probing beam current was 5.5 nA. The working distance of the instrument was 23 mm. The SEM images were used to locate positions for collecting the energy spectra and SAM images. The auto probe tracking was in effect during imaging to eliminate drifting due to instabilities in power and temperature, for example. HRTEM (JEM 2100F, JEOL, acceleration voltage = 200 kV) combined with EDX was also used to analyse the morphological features and chemical compositions of the inside and outside surfaces from cross-sections of the nanotrenches.

FORMATION OF Cr NANOWIRES AND Si NANOTRENCHES

Cr nanowires were formed by thermally evaporating Cr (target thicknesses of 4 and 8 nm) onto substrates, followed by lifting of the SiO_2 nanotrench mask in a diluted HF solution (H_2O:HF(50%) = 2:1 by volume) for ~1–3 min. Si nanotrenches were obtained by treating the SiO_2 nanotrench substrates with 45% KOH solution heated at 83 °C for 1 min. The substrate was then soaked in a diluted HF solution for 1 min to remove the SiO_2 nanotrench mask layer. Note that excess reaction of the KOH damages the SiO_2 mask, which is indicated visually by the generation of large numbers of H_2 bubbles from the substrate as well as by a change of surface colour to white.

Received 22 August 2006; accepted 9 January 2007; published 18 February 2007.

References

1. Shim, M., Javey, A., Kam, N. W. S. & Dai, H. Polymer functionalization for air-stable n-type carbon nanotube field effect transistors. *J. Am. Chem. Soc.* **123,** 11512–11513 (2001).
2. Javey, A., Guo, J., Wang, Q., Lundstrom, M. & Dai, H. Ballistic carbon nanotubes field effect transistors. *Nature* **424,** 654–657 (2003).
3. Kong, J. *et al.* Nanotube molecular wires as chemical sensors. *Science* **287,** 622–625 (2000).
4. Chen, R. J. *et al.* Carbon nanotubes as biocompatible materials and highly specific electronic biosensors. *Proc. Natl Acad. Sci. USA* **100,** 4984–4989 (2003).
5. Besteman, K., Lee, J.-O., Wiertz, F. G. M., Heering, H. A. & Dekker, C. Enzyme-coated carbon nanotubes as single-molecule biosensors. *Nano Lett.* **3,** 727–730 (2003).
6. Byon, H. R. & Choi, H. C. Network single-walled carbon nanotubes field effect transistors (SWNT-FETs) with increased Schottky contact area for highly sensitive biosensor applications. *J. Am. Chem. Soc.* **128,** 2188–2189 (2006).
7. Koc, R. & Cattamanchi, S. V. Synthesis of beta silicon carbide powders using carbon coated fumed silica. *J. Mater. Sci.* **33,** 2537–2549 (1998).
8. Choi, H. C. *et al.* Efficient formation of iron nanoparticle catalysts on silicon oxide by hydroxylamine for carbon nanotube synthesis and electronics. *Nano Lett.* **3,** 157–161 (2003).
9. Snow, E. S., Juan, W. H., Pang, S. W. & Campbell, P. M. Si nanostructures fabricated by anodic oxidation with an atomic force microscope and etching with an electron cyclotron resonance source. *Appl. Phys. Lett.* **66,** 1729–1731 (1995).
10. Li, J.-L. *et al.* Oxygen-driven unzipping of graphitic materials. *Phys. Rev. Lett.* **96,** 1761011–1761014 (2006).
11. Ajayan, P. M. & Yakobson, B. I. Oxygen breaks into carbon world. *Nature* **441,** 818–819 (2006).
12. Moulson, A. J. Reaction-bonded silicon nitride: its formation and properties. *J. Mater. Sci.* **14,** 1017–1051 (1979).
13. Yao, Y., Falk, L. K. L., Morjan, R. E., Nerushev, O. A. & Campbell, E. E. B. Synthesis of carbon nanotube films by thermal CVD in the presence of supported catalyst particles. Part I: the silicon substrate/nanotubes film interface. *J. Mater. Sci.* **15,** 533–543 (2004).
14. Homma, Y. *et al.* Role of transition metal catalysts in single-walled carbon nanotube growth in chemical vapor deposition. *J. Phys. Chem. B* **107,** 12161–12164 (2003).
15. Li, Y. *et al.* Growth of single-walled carbon nanotubes from discrete catalytic nanoparticles of various sizes. *J. Phys. Chem. B* **105,** 11424–11431 (2001).
16. Ural, A., Li, Y. & Dai, H. Electric-field-aligned growth of single-walled carbon nanotubes on surfaces. *App. Phys. Lett.* **81,** 3464–3466 (2002).
17. Hong, B. H. *et al.* Quasi-continuous growth of ultralong carbon nanotubes arrays. *J. Am. Chem. Soc.* **127,** 15336–15337 (2005).
18. Maruyama, S., Einarsson, E., Murakami, Y. & Edamura, T. Growth process of vertically aligned single-walled carbon nanotubes. *Chem. Phys. Lett.* **403,** 320–323 (2005).

Acknowledgements

This work was supported by the Basic Research Program of the KOSEF (R01-2004-000-10210-0), the Nano/Bio Science & Technology Program of MOST (M10536090000-05N3609-00000), the SRC/ERC Program (R11-2000-070-070020), and the Korean Research Foundation (MOEHRD, KRF-2005-005-J13103). The authors thank J. M. Buriak, D. Karpuzov and Shihong Xu for the SEM, SAM and AES experiments. Moon-Ho Jo and Jee-Eun Yang are thanked for Cr metal evaporations, and Joon Won Park and Il Hong Kim for ellipsometer measurements.
Supplementary information accompanies this paper on www.nature.com/naturenanotechnology.
Correspondence and requests for materials should be addressed to H.C.C.

Author contributions

H.C.C. and H.R.B. conceived and designed the experiments. H.R.B. performed experiments. H.C.C. and H.R.B. co-wrote the paper.

Competing financial interests

The authors declare that they have no competing financial interests.

A drawback of the Zhu *et al.* study, and of biophysical studies of HIV generally, should be noted. Under typical experimental conditions, most HIV particles are either not infectious or very slow to infect, and electron microscopy cannot distinguish between infectious and non-infectious particles. It could be that the only virus particles that do effectively infect are those with the highest number of spikes (up to 35 spikes per particle are described by Zhu *et al.*) and/or those particles with particular clustering patterns that are rarely seen.

Nonetheless, Zhu *et al.* provide some stunning images, particularly those of a tripod shape where a head composed mostly of three gp120 molecules balances on three gp41 legs, deduced by averaging data from a large number of SIV spikes. The image is not unlike depictions of menacing aliens that recur in films and books (for a selection try searching Google Image using 'tripods'). The legs are well separated, in contrast to most representations so far. This may help to explain the observation that the external parts of gp41 near the membrane are accessible to neutralizing antibodies, and will encourage vaccine designers to target these regions. The gp120 molecules sit atop the legs, with a sugar-coated face upwards and the variable loops along the side of the spike, probably restricting antibody access to the crucial CD4-binding site.

What next? Independent corroboration of the tripod structure from different strains and differently treated HIV and SIV preparations is highly desirable. Atomic force microscopy studies have given a different view of the HIV envelope spike[8], so determining which view is more likely in infectious particles is an important next step. Also, vaccine designers crave a high-resolution structure of an intact native HIV envelope trimer, and this is surely one of the most important unsolved structures in biomedicine. ■

Dennis R. Burton is in the Departments of Immunology and Molecular Biology, The Scripps Research Institute, 10550 North Torrey Pines Road, La Jolla, California 92037, USA.
e-mail: burton@scripps.edu

1. Zhu, P. *et al. Nature* **441,** 847–852 (2006).
2. Zwick, M. B., Saphire, E. O. & Burton, D. R. *Nature Med.* **10,** 133–134 (2004).
3. Kwong, P. D. *et al. Nature* **393,** 648–659 (1998).
4. Chen, B. *et al. Nature* **433,** 834–841 (2005).
5. Kwong, P. D. *et al. J. Virol.* **74,** 1961–1972 (2000).
6. Zhu, P. *et al. Proc. Natl Acad. Sci. USA* **100,** 15812–15817 (2003).
7. Yang, X., Kurteva, S., Ren, X. & Sodroski, J. *J. Virol.* **80,** 4388–4395 (2006).
8. Kuznetsov, Y. G., Victoria, J. G., Robinson, W. E. Jr & McPherson, A. *J. Virol.* **77,** 11896–11909 (2003).

MATERIALS SCIENCE

Oxygen breaks into carbon world

Pulickel M. Ajayan and Boris I. Yakobson

When oxygen atoms bind to a graphite surface, they fall into line and make bridges across carbon atoms. This is the spearhead of a chemical attack in which the atomic arrangement of solid carbon is torn apart.

What happens when we burn carbon? Combustion seems such a simple reaction, but at an atomic scale it is the result of several steps. When graphite burns, for example, an intermediate stage is the formation of a graphite oxide[1]. This process destabilizes the ordered arrangement of carbon atoms, so that cracks begin to form and the structure breaks up. Controlled oxidation reactions are useful for the preparation of very thin graphite flakes, or for chopping carbon nanotubes into shorter lengths, but the details of how oxygen attacks carbon bonds to break up the atomic structure of graphite have never been understood. Writing in *Physical Review Letters*, Je-Luen Li *et al.*[2] provide an explanation for this fundamental process.

The carbon atoms in graphite are arranged in a hexagonal lattice like a honeycomb, with each carbon bonded to three others, forming flat sheets held together by weak van der Waals forces. The bonds between the atoms are chemically inert, so unless there are flaws in the lattice, such as missing carbon atoms, the interaction of oxygen gas with a graphite surface is weak. During oxidation, the graphite oxide that forms is a complex structure[1] in which oxygen-containing groups are randomly attached to the honeycomb lattice. These groups, which can take part in varied surface chemistry, mainly attach at defects or edge-atom sites in the lattice, where the carbon atoms are not fully bonded to other atoms. So far so good, but how do the surface-bound oxygen-containing groups trigger the break-up of the carbon lattice, ultimately destroying the entire graphitic structure?

One kind of chemical group that forms on the graphite surface is known as an epoxy bridge, where a single oxygen atom bonds to two adjacent carbon atoms, forming a triangle. In their paper, Li *et al.*[2] describe how the stress generated by these epoxy bridges leads to unravelling of the graphite lattice. Each epoxy bridge is severely strained, because the geometry of the incorporated carbon atoms has changed. Where the bridged atoms were once only bound to other carbon atoms in a planar, hexagonal honeycomb arrangement, they are now bound to an oxygen atom sitting above the lattice surface, in place of a lattice carbon atom, and adopt an almost three-dimensional, distorted form. This new geometry doesn't fit well in the remaining lattice — it's like trying to fit a square peg into a round hole.

Mechanistically, the oxygen atom acts as a minuscule wedge, pushing apart the bridge's carbon atoms and stretching the carbon–carbon bond. The epoxy groups do not act individually, but cooperate. The authors' extensive calculations[2], based on density functional theory, show that side-by-side parallel positioning of the epoxy bridges is energetically favoured, so that they tend to line up on the graphite surface (Fig. 1). As a result, they collectively induce enough tension in the underlying lattice to break the native carbon bonds.

The feedback guiding such organized attachment of oxygen to graphite resembles generic brittle fracture, where the site of the next bond failure is determined by the existing crack as it propagates through the material. Having broken up carbon bonds, the bridging oxygen atoms go on to hold the fractured graphite sheet together, forming a seam between the separated lattice fragments. These fragments are held together at an angle to each other, to comply with the chemically preferred obtuse angle at the oxygen joints. The emerging network of such oxygen-zipped ridges results in the crumpling of a single graphite layer, known as a graphene sheet. This sheet flakes away from the stack of solid graphite, breaking the weak van der Waals forces that once bound it (Fig. 1).

The emerging picture of isolated epoxy groups falling into ranks, to take part in a well-orchestrated serial bond-breaking process, is rather appealing. But the kinetics require further explanation. Randomly bound epoxy groups are unaware of the energetic benefits of forming lines. The epoxy groups can only find such stable alignments as a result of rapid hopping around, but this is not easy to reconcile with the high energy barriers to such hopping. Further study is also required to determine exactly how visible faults or crack discontinuities emerge. Whatever the details may be, the lines of epoxy groups predetermine the tear pattern, like a perforation line directs the tear in a sheet of postage stamps. The resulting fault lines become clearly visible in optical microscope images of oxidized graphite[2].

A similar sequence of events can also be expected in the oxidation of carbon nanotubes. These share the same bonding as in graphite, except at the end caps where defects are present. Oxidation treatment in strong acids has led to the selective removal of end caps[3] and the breaking of long nanotubes into small pieces[4]. One would expect epoxy groups to line up circumferentially in a nanotube, leading to its transverse fracture into shorter segments, in a useful cutting process. On the other hand, uncontrolled oxidation can severely compromise the strength of nanotubes[5].

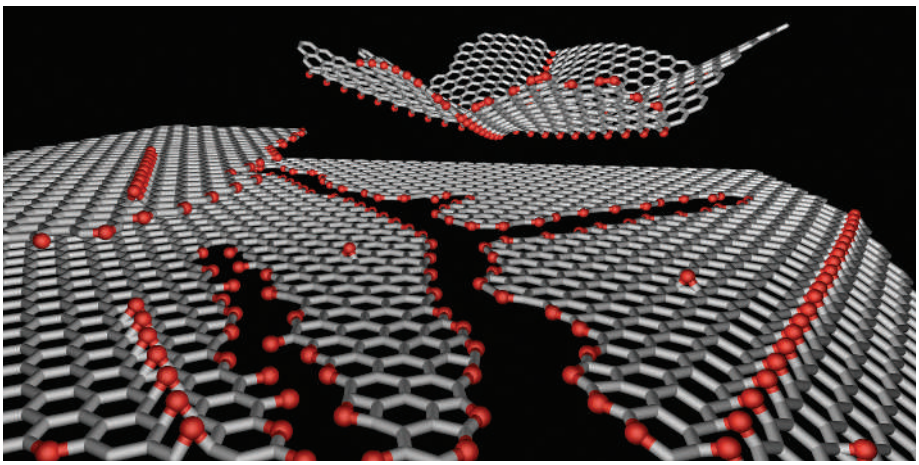

Figure 1 | Oxygen attack on graphite. Li *et al.*[2] show that when oxygen atoms (in red) bind to a graphite surface, they form two-legged epoxy bridges, which line up to lower their energy. This exerts a collective tension, breaking the underlying carbon–carbon bonds. Structural relaxation around the emerging ridges results in crumpling of the initially flat graphite sheets. This eases their separation, giving rise to distorted flakes of graphite, such as the one at the top of the figure. Faults along the oxygen trails lead to further mechanical fractures.

The paper by Li *et al.*[2] provides insight into the atomic-level mechanisms of oxidation in carbon. Graphite and its artefacts, such as carbon nanotubes, are materials with a wide range of uses, from lubrication to electronics. Controlled oxidative scission to extract nanoscale graphitic structures (for example, cut-to-size nanotubes[6] or nanosize graphene sheets[7]) from larger domains of these materials would be an extremely powerful technique for all sorts of applications. Understanding how oxygen breaks up the atomic structure of graphite could lead to a whole new area of nanotechnology based on nanoscale graphite origami[8]. ■

Pulickel M. Ajayan is in the Department of Materials Science and Engineering, Rensselaer Polytechnic Institute, Troy, New York 12180, USA.
e-mail: ajayan@rpi.edu
Boris I. Yakobson is in the Department of Mechanical Engineering and Materials Science, and the Department of Chemistry, Rice University, Houston, Texas 77005, USA.
e-mail: biy@rice.edu

1. He, H., Klinowski, J., Forster, M. & Lerf, A. *Chem. Phys. Lett.* **287,** 53–56 (1998).
2. Li, J.-L. *et al. Phys. Rev. Lett.* **96,** 176101 (2006).
3. Ajayan, P. M. & Iijima, S. *Nature* **361,** 333–334 (1993).
4. Liu, J. *et al. Science* **280,** 1253–1257 (1998).
5. Dumitrica, T., Hua, M. & Yakobson, B. I. *Proc. Natl Acad. Sci. USA* **103,** 6105–6109 (2006).
6. Ziegler, K. J. *et al. J. Am. Chem. Soc.* **127,** 1541–1547 (2005).
7. Berger, C. *et al. Science* **312,** 1191–1196 (2006).
8. Ebbesen, T. W. & Hiura, H. *Adv. Mater.* **7,** 582–586 (1995).

NEURODEGENERATION

Good riddance to bad rubbish

Daniel J. Klionsky

Autophagy — cellular 'self-eating' — can be induced by stress, but it also acts continuously in a housekeeping role, disposing of unwanted proteins. Can it protect against neurodegenerative diseases?

Alzheimer's, Parkinson's and Huntington's diseases are names we hear with a certain dread. These devastating illnesses, typically associated with ageing, result from the death of neurons. The cause of cell death is not known, but the onset of the disease symptoms is often accompanied by the appearance of large aggregates of particular proteins, such as Aβ in Alzheimer's, α-synuclein in Parkinson's, or huntingtin in Huntington's disease[1]. These are normal proteins — everyone has them — although their function is not always clear. For years, the consensus theory has been that the aggregated proteins lead directly to cell death. But perhaps the cellular housekeeper that should get rid of the proteins is at fault? There have been hints that autophagy may have a role in protecting against neurodegeneration, based on studies with human cell lines or animals with mutations that predispose them to these diseases[1]. In this issue, Komatsu *et al.*[2] (page 880) and Hara *et al.*[3] (page 885) provide the first genetic evidence that the housekeeping role of autophagy is essential for preventing neurodegenerative disease in healthy animals.

Protein aggregates have long been considered the major culprits in neurodegenerative disease because of the linear correlation between the age of disease onset and the time of aggregate appearance. Furthermore, certain mutated forms of the implicated proteins are more prone to aggregation and/or resistant to degradation, and result in earlier onset of neurological symptoms. Accordingly, many scientists in the field of neurodegeneration have focused on these mutated proteins and the accompanying large aggregates or 'inclusions' in cells.

Cells have several mechanisms to dispose of proteins when they misfold, become damaged or are no longer needed. One of the main degradation systems is the proteasome, a multi-subunit enzyme that breaks down proteins that have been tagged with ubiquitin. The proteasome only degrades unfolded, monomeric proteins, however, so it cannot handle protein aggregates. In addition, some of the mutant neuronal proteins are not good substrates for the proteasome.

The other principal degradation system is macroautophagy (which we shall refer to here as autophagy). The hallmark of this process is the formation of double-membrane bubble-like 'vesicles' that sequester portions of the cell's cytoplasm and deliver them to an organelle called the lysosome, where they are broken down (Fig. 1, overleaf). Autophagy can be induced by starvation and various hormonal stimuli[4]. Autophagic vesicles, or autophagosomes, can engulf entire organelles as well as the large aggregates generated by misfolded neuronal proteins. So, there is potential therapeutic value in being able to regulate autophagy to prevent or ameliorate some diseases. Recent data indicate, however, that the large protein aggregates are not the toxic species in these conditions[5,6]. Rather, the soluble or micro-aggregated forms may be the ones that cause cell death. What, then, is the role of autophagy, and its capacity to sequester large structures, in protecting against neurodegeneration?

Komatsu *et al.*[2] and Hara *et al.*[3] have engineered mice that lack the *Atg7* and *Atg5* autophagy genes, respectively. Both groups have used a genetic trick to delete the gene only from neural cells and only during later stages of embryogenesis, in order to bypass developmental defects that would arise from the elimination of the corresponding gene products constitutively (that is, in all cells throughout development). In both cases, mice lacking the autophagy genes develop symptoms of neurodegeneration, including neuronal cell death.

One reason these studies are of such significance is that they examine mice that are not genetically prone to neurodegenerative disease — the genes encoding the various neuronal proteins in these mice do not have the mutations associated with early onset of disease symptoms. These are healthy animals in which autophagy cannot be acting as an induced cytoprotective response to damaged proteins. This implies that the basal, housekeeping

INSTITUTE OF PHYSICS PUBLISHING NANOTECHNOLOGY
Nanotechnology **17** (2006) 5889–5894 doi:10.1088/0957-4484/17/23/029

Nanostructuring the graphite basal plane by focused ion beam patterning and oxygen etching

Artur Böttcher[1,4], Moritz Heil[1], Ninette Stürzl[1], Stefan S Jester[1], Sharali Malik[2], Fabián Pérez-Willard[3], Patrice Brenner[3], Dagmar Gerthsen[3] and Manfred M Kappes[1,2,4]

[1] Institut für Physikalische Chemie, Universität Karlsruhe, D-76131 Karlsruhe, Germany
[2] Institut für Nanotechnologie, Forschungszentrum Karlsruhe, D-76021 Karlsruhe, Germany
[3] Laboratorium für Elektronenmikroskopie, Universität Karlsruhe, D-76131 Karlsruhe, Germany

E-mail: artur.boettcher@chemie.uni-karlsruhe.de and manfred.kappes@chemie.uni-karlsruhe.de

Received 9 September 2006, in final form 20 October 2006
Published 16 November 2006
Online at stacks.iop.org/Nano/17/5889

Abstract
Ga^+ focused ion beam (FIB) patterning was used to structure highly oriented pyrolytic graphite surfaces with square, periodic arrays of amorphous carbon defects (mesh sizes: 300 nm–2 μm). Controlled oxygen etching of these arrays leads to matrices of uniform, orientationally aligned, nm-sized, hexagonal holes. The properties of the resulting hole assembly (hole depths and lateral hole dimensions) have been investigated by means of atomic force microscopy, scanning electron microscopy and FIB sectioning. The hole dimensions and uniformity both depend on the FIB parameters and etching conditions. Etching temperatures from 500 to 700 °C were applied. Initial etch rates of up to 10^6 C s^{-1} per individual hole were observed when using oxygen pressures of 200 mbar. For an etch temperature of 590 °C the rate of etching of individual holes was found to depend measurably on the inter-hole separation. This confirms that the associated reaction kinetics is mediated by the finite diffusion length of reactive oxygen species along the graphite basal plane. Prolonged etching results in hole–hole contact and generation of mesa arrays of controllable size and shape.

(Some figures in this article are in colour only in the electronic version)

1. Introduction

There are a number of ways to fabricate *randomly* distributed, flat-bottomed, nm-sized holes/pits in the basal plane of highly oriented pyrolytic graphite (HOPG). It is well known that one or a few monolayer (ML) deep nanoholes can be generated in graphite samples simply by heating in gaseous oxygen. The associated oxidation processes (generating CO and to a lesser extent CO_2) commence at 'natural' point defects and vacancies already present [1, 2]. Pits form because the horizontal etch rate along the basal plane is much faster than the vertical etch rate at the oxidation/etch temperatures used. Furthermore, there are slight differences among in-basal-plane etch rates along different crystallographic directions. Under the right experimental conditions this can lead to pits with hexagonal shapes, although more typically circular or irregular hole geometries are observed. Transmission electron microscopy (TEM), scanning electron microscopy (SEM), atomic force microscopy (AFM) and scanning tunnelling microscopy (STM) have been extensively used to investigate the corresponding pit growth kinetics [3, 4]. However, there remain many open questions with regard to the underlying oxidation mechanism [5].

Increasing the lateral density of randomly distributed etchable defects beyond that 'naturally' occurring in HOPG

[4] Authors to whom any correspondence should be addressed.

References

[1] Yang R T and Wong C 1981 *J. Chem. Phys.* **75** 4471
[2] Walker P L Jr, Vastola F J and Hart P J 1967 *Fundamentals of Gas–Surface Interactions* ed H Saltsburg, J N Smith Jr and M Rogers (New York: Academic) pp 307–17
[3] Yang R T 1984 *Chemistry and Physics of Carbon* vol 19, ed P L Walker Jr and P A Thrower (New York: Dekker) pp 163–210
[4] Hahn J R 2005 *Carbon* **43** 1506
[5] Schniepp H, Li J-L, McAllister M, Sai H, Herrera-Alonso M, Adamson D, Prud'homme R, Car R, Saville D and Aksay I 2006 *J. Phys. Chem.* B **110** 8535
[6] See e.g. Hahn J R and Kang H 2000 *Surf. Sci.* **446** L77 and references therein
[7] Bräuchle G 1996 *PhD Thesis* University of Karlsruhe (TH)
[8] Bräuchle G, Richard-Schneider S, Illig D, Rockenberger J and Kappes M M 1995 *Appl. Phys. Lett.* **67** 52
[9] Bräuchle G, Richard-Schneider S, Illig D, Beck R D, Schreiber H and Kappes M M 1996 *Nucl. Instrum. Methods* B **112** 105
[10] Pratontep S, Preece P, Xirouchaki C, Palmer R E, Sanz-Navarro C F, Kenny S D and Smith R 2003 *Phys. Rev. Lett.* **90** 055503
[11] Seminara L, Convers P, Monot R and Harbich W 2004 *Eur. Phys. J.* D **29** 49
[12] Perez A, Bardotti L, Prevel B, Jensen P, Treilleux M, Melinon P, Gierak J, Faini G and Mailly D 2002 *New J. Phys.* **4** 761
[13] Hannour A, Bardotti L, Prevel B, Bernstein E, Melinon P, Perez A, Geirak J, Bourhis E and Mailly D 2005 *Surf. Sci.* **594** 1
[14] Lu X, Huang H, Nemchuk N and Ruoff R S 1999 *Appl. Phys. Lett.* **75** 193
[15] Ziegler J F, Biersack J P and Littmark U 1985 *The Stopping and Range of Ions in Solids* (New York: Pergamon)
[16] Jester S *et al* 2006 in preparation
[17] Heil M *et al* 2006 in preparation
[18] Horton W S 1962 *Proc. 5th Carbon Conf.* (New York: Pergamon) pp 233–41
[19] Li J-L, Kudin K, McAllister M, Prud'homme R, Aksay I and Car R 2006 *Phys. Rev. Lett.* **96** 176101
[20] Chu X and Schmidt L D 1991 *Carbon* **29** 1251
[21] McKee D W and Spiro C L 1985 *Carbon* **23** 437
[22] Radovic L R and Walker P L Jr 1984 *Fuel Process. Technol.* **8** 149
[23] Stevens F, Kolodny L and Beebe T Jr 1998 *J. Phys. Chem.* B **102** 10799
[24] Burton W K, Cabrera N and Frank F C 1951 *Phil. Trans. R. Soc.* A **243** 299
[25] Lamoen D and Persson B N J 1998 *J. Chem. Phys.* **108** 3332
[26] Johansson S, Wong K, Zhdanov V P and Kasemo B 1999 *J. Vac. Sci. Technol.* A **17** 297
[27] Ghaemi H F, Thio T, Grupp D E, Ebbesen T W and Lezec H Z 1998 *Phys. Rev.* B **58** 6779

Available online at www.sciencedirect.com
ScienceDirect
Chemical Physics Letters 446 (2007) 109–114
CHEMICAL PHYSICS LETTERS
www.elsevier.com/locate/cplett

Investigations of NanoBud formation

Albert G. Nasibulin [a,*], Anton S. Anisimov [a], Peter V. Pikhitsa [b], Hua Jiang [c], David P. Brown [a], Mansoo Choi [b], Esko I. Kauppinen [a,c,*]

[a] NanoMaterials Group, Laboratory of Physics and Center for New Materials, Helsinki University of Technology, P.O. Box 1000, 02044 Espoo, Finland
[b] National CRI Center for Nano Particle Control, Institute of Advanced Machinery and Design, School of Mechanical and Aerospace Engineering, Seoul National University, Seoul 151-742, Republic of Korea
[c] VTT Biotechnology, P.O. Box 1000, 02044 VTT Espoo, Finland

Received 12 June 2007; in final form 7 August 2007
Available online 17 August 2007

Abstract

The formation of a novel hybrid material, NanoBuds, single-walled carbon nanotubes (CNTs) with covalently attached fullerenes was investigated in a ferrocene–carbon monoxide system. Fullerenes and CNTs were simultaneously formed by carbon monoxide disproportionation on the surface of iron particles in the presence of etching agents such as H_2O and CO_2. On the basis of parametric investigations and *in situ* sampling of the product from different locations in the reactor the mechanisms for NanoBud formation are discussed.

1. Introduction

Fullerenes and carbon nanotubes (CNTs) have attracted great interest from both fundamental and application points of view due to their remarkable physical and chemical properties [1–3]. Fullerenes and CNTs are usually produced in similar conditions and, in fact, were notoriously observed in a carbon arc discharge method [4] intended to produce only fullerenes [5]. In addition to arc discharge, another physical method for carbon vaporization, high-energy laser ablation, has also been shown to generate inhomogeneous mixtures of fullerenes and CNTs. Simultaneous formation of fullerenes and CNTs was also shown to occur in a HiPco reactor [6], where the produced fullerenes were separable in a solvent indicating weak bonding to the CNTs [7]. Transmission electron microscopy (TEM) observations often suggest that the surface of many CNTs is not clean and they are covered with some coating. It has been proposed that this coating can be converted to fullerenes in the intense electron beam of the microscope [8,9]. Also there have been several papers, where the presence of fullerene-like structures (or perhaps even fullerenes) on the surface of CNTs can be distinguished, but are not discussed [10–12].

There have been published very few experimental works attempting to combine fullerenes and CNTs into a single structure. Fullerene and CNT physical merging by means of solid phase mechanochemical reactions was proposed by Li et al. [13]. Theoretically, the combination of a fullerene and a CNT was first shown in a dynamic process of fullerene penetration into a CNT [14]. Recently, we have reported a one-step continuous process for the synthesis CNTs with covalently attached fullerenes [15]. This hybridization of fullerenes and CNTs resulted in the creation of a new material, NanoBuds, with interesting properties [15]. For instance, this structural arrangement of highly curved (chemically reactive) fullerenes and inert, but thermally and electrically conductive, CNTs, was shown to exhibit enhanced cold electron field emission properties [15]. In this paper, on the basis of parametric investigations and *in situ* sampling of the product from different locations in

* Corresponding authors. Address: NanoMaterials Group, Laboratory of Physics and Center for New Materials, Helsinki University of Technology, P.O. Box 1000, 02044 Espoo, Finland. Fax: +358 94567021 (A.G. Nasibulin).
E-mail addresses: albert.nasibulin@hut.fi (A.G. Nasibulin), esko.kauppinen@hut.fi (E.I. Kauppinen).

0009-2614/$ - see front matter © 2007 Elsevier B.V. All rights reserved.
doi:10.1016/j.cplett.2007.08.050

4. Conclusion

We have synthesized NanoBuds, single-walled CNTs covered by covalently bonded fullerenes, in a one-step continuous process by ferrocene vapor decomposition in a carbon monoxide atmosphere. Fullerenes and carbon nanotubes were simultaneously formed by carbon monoxide disproportionation on the surface of iron particles in the presence of etching agents H_2O and CO_2. Varying the introduced H_2O and CO_2 in the reactor revealed that the optimal reagent concentrations were between 45 and 245 ppm for H_2O and between 2000 and 6000 ppm for CO_2. Changing the temperature of the NanoBud synthesis at a introduced H_2O concentration showed its significant effect on the product morphology. *In situ* sampling of the product formed at different locations in the reactor showed that fullerenes were formed together with CNTs in the temperature interval between 885 and 945 °C. A mechanism of the fullerene formation during the CNT growth is proposed.

Acknowledgements

The authors thank Dr. S. Shandakov for fruitful discussions. Financial support from the Academy of Finland and the Creative Research Initiatives Program supported by the Korean Ministry of Science and Technology are gratefully acknowledged.

References

[1] M.S. Dresselhaus, G. Dresselhaus, P.C. Eklund, Science of Fullerenes and Carbon Nanotubes, Academic Press, San Diego, 1996.
[2] S. Reich, C. Thomsen, J. Maultzsch, Carbon Nanotubes, Wiley–VCH, Weinheim, 2004.
[3] S.V. Rotkin, S. Subramoney, Applied Physics of Carbon Nanotubes: Fundamentals of Theory, Optics and Transport Devices, Springer, Berlin, 2005.
[4] S. Iijima, Nature 354 (1991) 56.
[5] H.W. Kroto, J.R. Heath, S.C. O'Brien, R.F. Curl, R.E. Smalley, Nature 318 (1985) 162.
[6] S. Ramesh et al., J. Phys. Chem. B 107 (2003) 1360.
[7] A.K. Sadana et al., J. Phys. Chem. B 109 (2005) 4416.
[8] Y. Ando, X. Zhao, T. Sugai, M. Kumar, Mater. Today 7 (2004) 22.
[9] D. Golberg, Y. Bando, K. Kurashima, T. Sasaki, Carbon 37 (1999) 293.
[10] C.A. Dyke, J.M. Tour, Nano Lett. 3 (2003) 1215.
[11] Y.-H. Li et al., Small 2 (2006) 1026.
[12] M. Kumar, Y. Ando, Diam. Relat. Mater. 12 (2003) 1845.
[13] X. Li, L. Liu, Y. Qin, W. Wu, Z.-X. Guo, L. Dai, D. Zhu, Chem. Phys. Lett. 377 (2003) 32.
[14] Y. Zhao, Y. Lin, B.I. Yakobson, Phys. Rev. B 68 (2003) 233403.
[15] A.G. Nasibulin et al., Nat. Nanotechnol. 2 (2007) 156.
[16] A. Moisala, A.G. Nasibulin, D.P. Brown, H. Jiang, L. Khriachtchev, E.I. Kauppinen, Chem. Eng. Sci. 61 (2006) 4393.
[17] M. Monthioux, B.W. Smith, B. Burteaux, A. Claye, J.E. Fischer, D.E. Luzzi, Carbon 39 (2001) 1251.
[18] Je-L. Li, K.N. Kudin, M.J. McAllister, R.K. Prud'homme, I.A. Aksay, R. Car, Phys. Rev. Lett. 96 (2006) 176101.
[19] A.G. Nasibulin, D.P. Brown, P. Queipo, D. Gonzalez, H. Jiang, E.I. Kauppinen, Chem. Phys. Lett. 417 (2006) 179.
[20] A.G. Nasibulin et al., J. Nanosci. Nanotechnol. 6 (2006) 1233.
[21] D.P. Brown, A.G. Nasibulin, E.I. Kauppinen, J. Nanosci. Nanotechnol., accepted for publication.
[22] M. Audier, M. Coulon, L. Bonnetain, Carbon 21 (1983) 93.
[23] S. Herreyre, P. Gadelle, P. Moral, J.M.M. Millet, J. Phys. Chem. Solids 58 (1997) 1539.
[24] A.G. Nasibulin, P.V. Pikhitsa, H. Jiang, E.I. Kauppinen, Carbon 43 (2005) 2251.
[25] Y. Shibuta, S. Maruyama, Physica B 323 (2002) 187.
[26] F. Ding, A. Rosén, K. Bolton, Chem. Phys. Lett. 393 (2004) 309.
[27] J.-Y. Raty, F. Gygi, G. Galli, Phys. Rev. Lett. 95 (2005) 096103.
[28] A. Rasheed, J.Y. Howe, M.D. Dadmun, Carbon 45 (2007) 1072.
[29] R. Tamura, M. Tsukada, Phys. Rev. B 49 (1994) 7697.

Articles

Single Sheet Functionalized Graphene by Oxidation and Thermal Expansion of Graphite

Michael J. McAllister,[†] Je-Luen Li,[‡,§,||] Douglas H. Adamson,[§] Hannes C. Schniepp,[†] Ahmed A. Abdala,[†,⊥] Jun Liu,[⊗,○] Margarita Herrera-Alonso,[†] David L. Milius,[†] Roberto Car,[‡,§] Robert K. Prud'homme,[†] and Ilhan A. Aksay*[,†]

Department of Chemical Engineering, Department of Chemistry, and Princeton Institute for the Science and Technology of Materials, Princeton University, Princeton, New Jersey 08544, and Sandia National Laboratories, Albuquerque, New Mexico 87185

Received December 26, 2006. Revised Manuscript Received February 6, 2007

A detailed analysis of the thermal expansion mechanism of graphite oxide to produce functionalized graphene sheets is provided. Exfoliation takes place when the decomposition rate of the epoxy and hydroxyl sites of graphite oxide exceeds the diffusion rate of the evolved gases, thus yielding pressures that exceed the van der Waals forces holding the graphene sheets together. A comparison of the Arrhenius dependence of the reaction rate against the calculated diffusion coefficient based on Knudsen diffusion suggests a critical temperature of 550 °C which must be exceeded for exfoliation to occur. As a result of their wrinkled nature, the functionalized and defective graphene sheets do not collapse back to graphite oxide but are highly agglomerated. After dispersion by ultrasonication in appropriate solvents, statistical analysis by atomic force microscopy shows that 80% of the observed flakes are single sheets.

Introduction

Graphene, the basal plane of graphite, is composed of a honeycomb arrangement of carbon atoms and is the basis of carbon nanotubes (CNTs).[1,2] Graphene single sheets are expected to have tensile modulus and ultimate strength values similar to those of single wall carbon nanotubes (SWCNTs)[3] and are also electrically conducting.[4] Much like SWCNTs,[5] graphene sheets serve as fillers for the enhancement of mechanical[6] and electrical properties[7] in composite materials. Recent studies in which single sheets of graphene have been prepared by the removal of one sheet at a time by a "Scotch tape" method have shown promising electrical properties that could be useful for developing novel electronic devices.[4,8−12] Motivated by the promise of graphene as an alternative to SWCNTs, in a recent study[13] we reported a method to produce functionalized single graphene sheets (FGSs) in bulk quantities through thermal expansion of graphite oxide (GO). In this report, we provide a detailed analysis of the expansion mechanism and a detailed characterization of the resultant material.

* Corresponding author: e-mail iaksay@princeton.edu.
† Department of Chemical Engineering, Princeton University.
‡ Department of Chemistry, Princeton University.
§ Princeton Institute for the Science and Technology of Materials, Princeton University.
|| Current address: Institute of Atomic and Molecular Sciences, Academia Sinica, Taipei 10617, Taiwan.
⊥ Current address: Department of Chemical Engineering, The Petroleum Institute, POB 2533, Abu Dhabi, United Arab Emirates.
⊗ Sandia National Laboratories.
○ Current address: Pacific Northwest National Laboratory, Richland, Washington 99352.

(1) Iijima, S. *Nature* **1991**, *354*, 56.
(2) Ajayan, P. M.; Iijima, S. *Nature* **1993**, *361*, 333.
(3) Ab initio calculations by Je-Luen Li and Roberto Car (Princeton University) showed that the stress−strain behaviors of graphene sheets and SWCNTs are very similar. The calculated Young's modulus is 1.01 TPa for graphene sheet and 0.94−0.96 TPa for SWCNT provided the same graphene sheet thickness (0.34 nm) is used.
(4) Novoselov, K. S.; Geim, A. K.; Morozov, S. V.; Jiang, D.; Zhang, Y.; Dubonos, S. V.; Grigorieva, I. V.; Firsov, A. A. *Science* **2004**, *306*, 666.
(5) Ramanathan, T.; Liu, H.; Brinson, L. C. *J. Polym. Sci., Part B: Polym. Phys.* **2005**, *43*, 2269.
(6) Ramanathan, T.; Abdala, A. A.; Stankovich, S.; Dikin, D. A.; Herrera-Alonso, M.; Piner, R. D.; Adamson, D. H.; Liu, J.; Chen, X.; Ruoff, R. S.; Nguyen, S. T.; Aksay, I. A.; Prud'homme, R. K.; Brinson, L. C., unpublished.
(7) Stankovich, S.; Dikin, D. A.; Dommett, G. H. B.; Kohlhaas, K. M.; Zimney, E. J.; Stach, E. J.; Piner, R. D.; Nguyen, S. T.; Ruoff, R. S. *Nature* **2006**, *442*, 282.
(8) Duplock, E. J.; Scheffler, M.; Lindan, P. J. D. *Phys. Rev. Lett.* **2004**, *92*, 225502.
(9) Novoselov, K. S.; Jiang, D.; Schedin, F.; Booth, T. J.; Khothevich, V. V.; Morozov, S. V.; Geim, A. K. *Proc. Natl. Acad. Sci. U.S.A.* **2005**, *102*, 10451.
(10) Zhang, Y.; Tan, Y. W.; Stormer, H. L.; Kim, P. *Nature* **2005**, *438*, 201.
(11) Zhang, Y.; Small, J. P.; Amori, M. E. S.; Kim, P. *Phys. Rev. Lett.* **2005**, *94*, 176803.
(12) Novoselov, K. S.; Geim, A. K.; Morozov, S. V.; Jiang, D.; Katsnelson, M. I.; Grigorieva, I. V.; Dubonos, S. V.; Firsov, A. A. *Nature* **2005**, *438*, 197.
(13) Schniepp, H. C.; Li, J.-L.; McAllister, M. J.; Sai, H.; Herrera-Alonso, M.; Adamson, D. H.; Prud'homme, R. K.; Car, R.; Saville, D. A.; Aksay, I. A. *J. Phys. Chem. B* **2006**, *110*, 8535.

10.1021/cm0630800 CCC: $37.00
Published on Web 05/25/2007

K_α radiation, $\lambda = 1.5406$ Å, 9009 New Trails Dr., The Woodlands, TX 77381-5209).

Thermal exfoliation of GO as prepared above was achieved by placing GO (200 mg) into a 25-mm i.d., 1.3-m long quartz tube that was sealed at one end. The other end of the quartz tube was closed using a rubber stopper. An argon inlet was then inserted through the rubber stopper. The sample was flushed with argon for 10 min, and the quartz tube was quickly inserted into a Lindberg tube furnace preheated to 1050 °C and held in the furnace for 30 s.

Oxidized graphite samples were examined by simultaneous thermal gravimetric analysis (TGA) and differential scanning calorimetry (DSC; STA 449 C Jupiter, Erich Netzsch GmbH & Co., Holding KG, D-95100 Selb, Germany). The differential scanning calorimeter was calibrated by a set of standards with known temperatures and enthalpies (In, Sn, Bi, Zn, CsCl). The thermal analysis unit was coupled with a Fourier transform infrared (FTIR) spectrometer for evolved gas analysis (Thermo Nicolet Nexus 670, Thermo Electron Corp., Waltham, MA 02451).

Characterization of Graphite, GO, and FGS. Transmission electron microscope imaging of graphite, GO, and FGS was performed on a JEOL 2010 FEG microscope at 200 keV to characterize especially the variations in the stacking of graphene sheets. The transmission electron microscopy (TEM) samples were prepared by dispensing a small amount of dry powder on 200 mesh copper TEM grids covered with thin amorphous carbon films. The *d*-spacing was calibrated against the interplanar spacing of graphite.

Graphite, GO, and FGS were also characterized by scanning electron microscopy (SEM; Tescan 5130MM, Libusina tr. 21, 62300 Brno, Czech Republic) to determine particle size and microscopic features. SEM samples of GO were prepared by placing a 1 cm-diameter drop of dilute GO suspension on a 1 × 1 cm section of silicon wafer and allowing the solvent to evaporate. The wafer was then attached to an aluminum sample holder with conductive carbon adhesive. The samples were coated with 2−3 nm of iridium to ensure good conductivity. FGS samples for SEM imaging were prepared by applying the powder directly to a carbon adhesive tape.

Imaging of FGS by atomic force micrsocopy (AFM; Multimode, Nanoscope IIIa, Veeco Instruments, Inc., Santa Barbara, CA) was performed with special emphasis on sheet thickness, morphological features, and lateral dimensions. The cantilevers were Veeco NP-S type (gold-coated, oxide-sharpened silicon nitride, force constant $k = 0.58$ N/m, radius of curvature $r = 20$ nm). For the most accurate determination of the sheet thickness, contact mode was applied and topography sections across a sheet, starting and ending on a highly oriented pyrolytic graphite (HOPG) substrate, were taken, following the fast scanning direction. Samples of FGS were prepared by loading a 50 mL flask with 4 mg of graphene and 40 mL of dimethylformamide (DMF) as the dispersion medium. The suspension was ultrasonicated for 30 min. This suspension was diluted to a concentration of 0.02 mg/mL. The final suspension was spin-coated at 5000 rpm on a freshly cleaved surface of HOPG.

Surface area was measured using the Brunauer, Emmett, and Teller (BET)[40] method (Micromeritics Gemini V, One Micromeritics Drive, Norcross, GA 30093) and also in suspension using UV−vis spectroscopy with methylene blue (MB) dye as a probe. Water is the solvent of choice for MB; however, it is a poor dispersant for FGS. Ethanol is a much better dispersant for the FGS suspension but gives a less well-defined peak for MB absorption. We therefore used a combination of the two solvents to make our measurements.

In the MB technique, the surface area measurements were taken by first adding a known mass of FGS to a flask. An amount of MB equal to at least 1.5 times the amount required to cover the theoretical surface area of graphene (2630 m^2/g)[38] was then added. Ethanol was added, followed by sonication with stirring for 1.5 h. The ethanol was then evaporated, and the free MB was redissolved by a known quantity of water. The concentration of MB was subsequently determined by UV−vis spectroscopy relative to standard concentrations. The measurements were made at $\lambda = 298$ nm. Although the reported values of λ_{max} in the literature vary,[41−44] this value is significantly lower than those normally reported, and we expect this was caused by the use of ethanol during the process. The literature value of 2.54 m^2 of surface covered per mg of MB adsorbed was the basis for our calculations.[41] Recent literature reports tend to use a value corresponding to a coverage of 1.30 nm^2 per molecule of MB.[42] However, depending on the assumptions made, the surface coverage of a single MB molecule is reported to range from 1.30 nm^2 for molecules laying flat to 0.66 nm^2 for tilted molecules.[43] For graphite-based samples, flat monolayer coverage is expected.[43,44]

Results and Discussion

Mechanism of Exfoliation. For a successful exfoliation process, we have found it necessary to first increase the *c*-axis spacing by oxidation to 0.7 nm and completely eliminate the 0.34 nm graphite interlayer spacing (Figure 1).[13] The reaction time required to achieve the appropriate level of oxidation for the elimination of the 0.34 nm graphite peak depended on the starting flake size. The reaction progress was monitored by withdrawing aliquots from the reaction vessel to be characterized by XRD. The results from studies of two different size flakes, 400 and 45 μm diameter, are shown in Figure 1. From the XRD data, it can be seen that the reaction proceeds more quickly for the 45 μm plates.

During the oxidation process both the 400 and 45 μm graphite flakes break down into smaller GO flakes with sizes on the order of 10 μm in diameter as shown in Figure 2. This final size does not depend on the initial size of the graphite flakes. The oxidative breakup may be facilitated by existing defects as well as a previously proposed cooperative unzipping mechanism.[45] Reducing the starting flake size allows for faster, more reliable oxidation reactions without a significant difference in the final GO flake size.

To determine the composition of the evolved gases that cause the rapid expansion, a series of TGA/DSC experiments were performed where the outlet gas is analyzed by FTIR. A typical TGA/DSC scan of GO along with the FTIR scans performed at varying temperatures is shown in Figure 3. The heating rate had to be kept at or below 1 °C/min to avoid exfoliating the material during the scan. Faster heating rates produce deflagration sufficiently powerful to remove the pan lid and most of the sample from the pan, resulting in inaccurate scans. Small amounts of water are lost during the initial heating stage. At 200 °C, there is a dramatic mass

(40) Brunauer, S.; Emmett, P. H.; Teller, E. *J. Am. Chem. Soc.* **1938**, *60*, 309−19.
(41) Rubino, R. S.; Takeuchi, E. S. *J. Power Sources* **1999**, *81*, 373.
(42) Yukselen, Y.; Kaya, A. *J. Geotech. Geoenviron. Eng.* **2006**, *132*, 931.
(43) Pakhovchishin, S. V.; Chernysh, I. G.; Gritsenko, V. F. *Colloid Journal of the USSR* **1991**, *53*, 245.
(44) Sagara, T.; Niki, K. *Langmuir* **1993**, *9*, 831−838.
(45) Li, J.-L.; Kudin, K. N.; McAllister, M. J.; Prud'homme, R. K.; Aksay, I. A.; Car, R. *Phys. Rev. Lett.* **2006**, *96*, 176101.

Multiscale Imaging and Tip-Scratch Studies Reveal Insight into the Plasma Oxidation of Graphite

J. I. Paredes,* A. Martínez-Alonso, and J. M. D. Tascón

Instituto Nacional del Carbón, CSIC, Apartado 73, 33080 Oviedo, Spain

Received March 16, 2007. In Final Form: May 22, 2007

The plasma oxidation process of highly oriented pyrolytic graphite (HOPG) has been investigated through a combination of multiscale (micrometric to atomic) imaging by atomic force and scanning tunneling microscopies (AFM/STM) and STM tip-scratching of the HOPG substrate. Complementary information was obtained by Raman spectroscopy and X-ray photoelectron spectroscopy (XPS). Repetitive imaging of the same HOPG location following a series of consecutive plasma treatments allowed an accurate determination of the plasma etch rates along both the *a* and *c* crystallographic directions of the graphite lattice. The etch rates were typically in the range of a few nm per min along the *a* axis, and the equivalent of 1−6 graphene layers per min along the *c* axis. The results pointed to the existence of two main plasma etching regimes, related to short (<20−30 min) and long (≥30 min) treatment times. This was inferred not only from the measured plasma etch rates but also from the observation of fundamental differences in the atomic-scale surface structure of the plasma-treated HOPG samples, and from the general mechanical behavior of the materials under the action of the AFM tip. In particular, atomic-scale STM imaging suggested a change from a defected, but essentially graphitic, surface in the first regime to an amorphous carbon surface in the second regime. Together with AFM and STM, Raman spectroscopy and XPS provided a consistent picture of the surface structure and chemistry of the plasma-modified HOPG in the two regimes. The implications of these results as well as the possible mechanism that drives the plasma etching process in the two regimes are discussed.

1. Introduction

The surface modification of graphite presents particular interest from a fundamental science perspective as well as from the point of view of practical applications. In the former case, surface-modified graphite has proved to be a suitable model system for both experimental and theoretical studies related to a wide variety of issues. These include carbon combustion,[1−4] the performance of structural materials employed in spacecraft,[5−7] the templated growth of nanostructures,[8] the electrochemistry of carbon materials,[9] the investigation of nanoparticle−substrate interactions[10−13] and of carbon-supported catalysts,[14,15] or the adsorption of molecules on carbon surfaces.[16−18] In the realm of direct applications, graphite is used, for instance, as the negative electrode in lithium ion batteries, where different types of surface modification of the graphitic anode are currently being investigated with the aim of improving the efficiency of such devices.[19,20] Another area of interest has emerged very recently with the advent of methodologies that allow the preparation and processing of very thin graphite flakes, with thicknesses ranging from several nanometers down to the single graphene level.[21,22] One of the potential applications proposed for this two-dimensional counterpart of graphite is as a filler in composite materials.[23−26] Again in this case, an appropriate functionalization of the graphite flake surface is thought to be necessary in order to achieve composites with optimum performance.[24−26]

In many of the examples mentioned above, oxidation was used as the basic method to modify and manipulate the surface of graphite. Thus, graphite oxidation is considered a topic of scientific and technological relevance.[1−7,27] In particular, oxidation by plasmas is rather attractive, since it offers several advantages over other types of oxidation (e.g., electrochemical, thermal, or wet chemical oxidation): it is a nonpolluting process,

* Corresponding author. Telephone number: (+34) 985 11 90 90. Fax number: (+34) 985 29 76 62. E-mail address: paredes@incar.csic.es.

(1) Chang, H.; Bard, A. J. *J. Am. Chem. Soc.* **1991**, *113*, 5588−5596.
(2) Tandon, D.; Hippo, E. J.; Marsh, H.; Sebok, E. *Carbon* **1997**, *35*, 35−44.
(3) Lee, S. M.; Lee, Y. H.; Hwang, Y. G.; Hahn, J. R.; Kang, H. *Phys. Rev. Lett.* **1999**, *82*, 217−220.
(4) Hahn, J. R. *Carbon* **2005**, *43*, 1506−1511.
(5) Ngo, T.; Snyder, E. J.; Tong, W. M.; Williams, R. S.; Anderson, M. S. *Surf. Sci.* **1994**, *314*, L817−L822.
(6) Kinoshita, H.; Umeno, M.; Tagawa, M.; Ohmae, N. *Surf. Sci.* **1999**, *440*, 49−59.
(7) Nicholson, K. T.; Minton, T. K.; Sibener, S. J. *J. Phys. Chem. B* **2005**, *109*, 8476−8480.
(8) Liu, Y.; Zhang, Z.; Wells, M. C.; Beebe, T. P. *Langmuir* **2005**, *21*, 8883−8891.
(9) Davies, T. J.; Hyde, M. E.; Compton, R. G. *Angew. Chem., Int. Ed.* **2005**, *44*, 5121−5126.
(10) Palmer, R. E.; Pratontep, S.; Boyen, H.-G. *Nat. Mater.* **2003**, *2*, 443−448.
(11) Yang, D.-Q.; Sacher, E. *Chem. Mater.* **2006**, *18*, 1811−1816.
(12) Yang, D.-Q.; Zhang, G.-X.; Sacher, E.; José-Yacamán, M.; Elizondo, N. *J. Phys. Chem. B* **2006**, *110*, 8348−8356.
(13) Akola, J.; Häkkinen, H. *Phys. Rev. B* **2006**, *74*, 165404.
(14) Song, Z.; Cai, T.; Hanson, J. C.; Rodriguez, J. A.; Hrbek, J. *J. Am. Chem. Soc.* **2004**, *126*, 8576−8584.
(15) Kibsgaard, J.; Lauritsen, J. V.; Lægsgaard, E.; Clausen, B. S.; Topsøe, H.; Besenbacher, F. *J. Am. Chem. Soc.* **2006**, *128*, 13950−13958.
(16) Kwon, S.; Vidic, R.; Borguet, E. *Carbon* **2002**, *40*, 2351−2358.
(17) Orasanu-Gourlay, A.; Bradley, R. H. *Adsorpt. Sci. Technol.* **2006**, *24*, 117−130.
(18) Wang, X.-L.; Lu, Z.-Y.; Li, Z.-S.; Sun, C.-C. *Langmuir* **2007**, *23*, 802−808.
(19) Zhang, S. S.; Xu, K.; Jow, T. R. *J. Power Sources* **2004**, *129*, 275−279.
(20) Doi, T.; Takeda, K.; Fukutsuka, T.; Iriyama, Y.; Abe, T.; Ogumi, Z. *Carbon* **2005**, *43*, 2352−2357.
(21) Novoselov, K. S.; Jiang, D.; Schedin, F.; Booth, T. J.; Khotkevich, V. V.; Morozov, S. V.; Geim, A. K. *Proc. Natl. Acad. Sci. U.S.A.* **2005**, *102*, 10451−10453.
(22) Niyogi, S.; Bekyarova, E.; Itkis, M. E.; McWilliams, J. L.; Hamon, M. A.; Haddon, R. C. *J. Am. Chem. Soc.* **2006**, *128*, 7720−7721.
(23) Lu, J.; Weng, W.; Chen, X.; Wu, D.; Wu, C.; Chen, G. *Adv. Funct. Mater.* **2005**, *15*, 1358−1363.
(24) Stankovich, S.; Dikin, D. A.; Dommett, G. H. B.; Kohlhaas, K. M.; Zimney, E. J.; Stach, E. A.; Piner, R. D.; Nguyen, S. T.; Ruoff, R. S. *Nature* **2006**, *442*, 282−286.
(25) Schniepp, H. C.; Li, J.-L.; McAllister, M. J.; Sai, H.; Herrera-Alonso, M.; Adamson, D. H.; Prud'homme, R. K.; Car, R.; Saville, D. A.; Aksay, I. A. *J. Phys. Chem. B* **2006**, *110*, 8535−8539.
(26) Hung, M.-T.; Choi, O.; Ju, Y. S.; Hahn, H. T. *Appl. Phys. Lett.* **2006**, *89*, 023117.
(27) Li, J.-L.; Kudin, K. N.; McAllister, M. J.; Prud'homme, R. K.; Aksay, I. A.; Car, R. *Phys. Rev. Lett.* **2006**, *96*, 176101.

10.1021/la700780k CCC: $37.00
Published on Web 07/12/2007

it is potentially scalable, and reaction times are shorter.[28] As various recent examples demonstrate, plasma oxidation is a useful approach to enhance and/or fine-tune the surface properties not only of graphite[11,16] but also of other sp^2-based carbon materials of interest, such as carbon nanotubes[29−31] and activated carbon fibers.[32−34]

Nonetheless, our current understanding of the plasma oxidation process of carbon materials is still relatively limited compared to the other types of oxidation. Previous studies on graphite have mostly established the main morphological changes on the micrometer and nanometer scales induced by oxygen plasma exposure.[35−38] In another study, atomic-scale scanning tunneling microscopy (STM) was employed to reveal the very initial stages of microwave plasma oxidation of graphite.[39] It was concluded that the attack starts with the creation of monatomic vacancies on the graphite surface that subsequently develop into multiatomic vacancies. However, several important questions of plasma oxidation were not addressed in this or any other earlier study. For example, the plasma etching rates along both the *a* and *c* directions of the graphite lattice, i.e., along directions parallel and perpendicular to the basal plane, respectively, have not yet been compared or determined. Accurate knowledge of these etch rates could be useful, for instance, in the patterning of ultrathin graphite films, which are actively investigated at present as promising candidates for applications in nanoscale electronics.[40,41] Another unresolved question is how etching proceeds on the atomic scale in later stages of plasma oxidation. This point is not a trivial one, considering that plasmas are nonequilibrium media, and therefore the observations made in the very early stages of attack[39] might not apply at longer etching times, which are more representative of practical treatments.

In this work, we address these and other issues of the plasma oxidation of graphite by mainly employing atomic force microscopy (AFM) and STM at scales ranging from the micrometer level down to the atomic scale. Moreover, to answer some of the posed questions, we have used an STM tip-scratch method that serves two principal purposes: first, it creates marks on the graphite surface that allow the repetitive location and imaging of the same spot after consecutive plasma treatments of a given sample. Second, this procedure also generates features on the graphite surface with adequate dimensions so as to extract useful information about the plasma process. Although other tip-scratch methods based on scanning probe microscopy have been previously reported, e.g., for the determination of polymer film thickness with AFM,[42] to the best of our knowledge this is the first time that such an approach is applied to follow and extract information about any type of surface modification of graphite or any other material. In addition to the AFM and STM studies, complementary information on the surface structure and chemistry of the plasma-treated graphite was obtained by Raman and X-ray photoelectron spectroscopies.

2. Experimental Section

The graphite samples used in the present study were grade ZYH highly oriented pyrolytic graphite (HOPG), obtained from Advanced Ceramics Corp. (Cleveland, OH). Just before any manipulation, the HOPG specimens were cleaved in air to obtain fresh, pristine surfaces. Oxygen plasma treatments of HOPG were carried out in a Technics Plasma 200-G apparatus (Kircheim bei München, Germany). The plasma was activated by 2.45 GHz microwave (MW) radiation, which in turn was generated with a magnetron. The MW radiation was transferred through a waveguide from the magnetron to the quartz chamber where the plasma was created and the HOPG samples were placed. The treatments were accomplished at a MW power of 100 W and at a working pressure in the chamber of 1.0 mbar. O_2 (99.999% pure) was used as the plasma gas. HOPG samples were exposed to the oxygen plasma for typical periods of 10 or 30 min and then analyzed. Afterward, the same HOPG specimen was submitted to an additional plasma treatment and analyzed again. This process was usually repeated several times, so at the end the sample had been consecutively treated and analyzed up to 5 times.

Following each individual plasma treatment, the HOPG samples were investigated by AFM/STM under ambient conditions (relative humidity ∼40%, temperature ∼22−24 °C) both at random surface locations and repeatedly at given spots that were predefined on the untreated HOPG surface by an STM tip-scratch method. The STM tip-scratching of pristine HOPG as well as the AFM/STM imaging of the plasma-treated material were carried out in a Nanoscope IIIa Multimode system, from Veeco Instruments (Santa Barbara, CA). To create predefined spots by tip-scratching, a Pt/Ir (80/20) STM tip was approached to the freshly cleaved HOPG surface in discrete (∼100 nm) steps while monitoring the tip apex/sample region with an optical microscope coupled to the AFM/STM apparatus. In this way, the tip was allowed to contact and scratch the HOPG surface, and it was normally retracted as soon as damage to the material could be observed with the optical microscope. This process mostly led to the exfoliation of an area of the HOPG surface with a lateral size of several micrometers and a depth in the range from several to a few tens of nm. The tip-scratched (exfoliated) area could then be easily located with the optical microscope for repeated AFM/STM visualization.

For imaging of the plasma-treated samples by AFM, the tapping mode of operation was preferred over the contact mode. Experiments in which the same area was scanned first in the contact mode and then in the tapping mode indicated that imaging with the former could easily damage/exfoliate the plasma-oxidized HOPG samples, particularly those treated at shorter times (e.g., 10 min). Damage to the samples could be minimized to an acceptable level with the tapping mode, although it could not be completely avoided in some cases, as will be shown later. For this reason, the AFM images shown in this work correspond to the tapping mode. The tapping mode images were recorded with rectangular silicon cantilevers, which had spring constants of about 40 N m^{-1} and resonance frequencies around 250 kHz. The contact mode was used for imaging and for the measurement of tip−sample adhesion forces through the recording of force-displacement curves. In this case, triangular silicon nitride cantilevers with nominal spring constants of 0.12 N m^{-1} were employed. The adhesion forces were calculated as the average of a few hundred individual measurements at random surface locations.

(28) Felten, A.; Bittencourt, C.; Pireaux, J. J.; Van Lier, G.; Charlier, J. C. *J. Appl. Phys.* **2005**, *98*, 074308.
(29) Han, S. S.; Kim, H. S.; Han, K. S.; Lee, J. Y.; Lee, H. M.; Kang, J. K.; Woo, S. I.; van Duin, A. C. T.; Goddard, W. A., III *Appl. Phys. Lett.* **2005**, *87*, 213113.
(30) Felten, A.; Bittencourt, C.; Pireaux, J. J. *Nanotechnology* **2006**, *17*, 1954−1959.
(31) Rawat, D. S.; Taylor, N.; Talapatra, S.; Dhali, S. K.; Ajayan, P. M.; Migone, A. D. *Phys. Rev. B* **2006**, *74*, 113403.
(32) Park, S.-J.; Kim, B.-J. *J. Colloid Interface Sci.* **2004**, *275*, 590−595.
(33) Korovchenko, P.; Renken, A.; Kiwi-Minsker, L. *Catal. Today* **2005**, *102−103*, 133−141.
(34) Tang, S.; Lu, N.; Wang, J. K.; Ryu, S.-K.; Choi, H.-S. *J. Phys. Chem. C* **2007**, *111*, 1820−1829.
(35) Joshi, A.; Nimmagadda, R. *J. Mater. Res.* **1991**, *6*, 1484−1490.
(36) You, H.-X.; Brown, N. M. D.; Al-Assadi, K. F. *Surf. Sci.* **1993**, *284*, 263−272.
(37) Lu, X.; Huang, H.; Nemchuk, N.; Ruoff, R. S. *Appl. Phys. Lett.* **1999**, *75*, 193−195.
(38) Paredes, J. I.; Martínez-Alonso, A.; Tascón, J. M. D. *J. Mater. Chem.* **2000**, *10*, 1585−1591.
(39) Paredes, J. I.; Martínez-Alonso, A.; Tascón, J. M. D. *Langmuir* **2002**, *18*, 4314−4323.
(40) Novoselov, K. S.; Geim, A. K.; Morozov, S. V.; Jiang, D.; Zhang, Y.; Dubonos, S. V.; Grigorieva, I. V.; Firsov, A. A. *Science* **2004**, *306*, 666−669.
(41) Berger, C.; Song, Z.; Li, X.; Wu, X.; Brown, N.; Naud, C.; Mayou, D.; Li, T.; Hass, J.; Marchenkov, A. N.; Conrad, E. H.; First, P. N.; de Heer, W. A. *Science* **2006**, *312*, 1191−1196.
(42) Ton-That, C.; Shard, A. G.; Bradley, R. H. *Langmuir* **2000**, *16*, 2281−2284.

Role of the Epoxy Group in the Heterogeneous CO_2 Evolution in Carbon Oxidation Reactions

Astrid Sánchez and Fanor Mondragón*

Institute of Chemistry, University of Antioquia, A.A. 1226 Medellín, Colombia

Received: September 1, 2006; In Final Form: October 28, 2006

A density functional theory study was carried out to evaluate different possibilities of heterogeneous CO_2 desorption in combustion/gasification reactions. First, we investigated the heterogeneous CO_2 evolution induced as a secondary reaction caused by the CO readsorption on an oxidized surface, which produces a carbonate-like surface complex. This functional group was found to decompose as CO_2 with an activation energy of 60 kcal/mol. Another possibility for heterogeneous CO_2 formation during char combustion or gasification is through the molecular O_2 chemisorption on a carbon active site of an oxidized graphene layer. The peroxy complex thus formed undergoes rearrangement into a dioxiranyl complex, C(2O). This complex can evolve as CO_2 with an activation energy of 48 kcal/mol. The CO_2 desorption is facilitated by the presence of an epoxy complex near the edge of the graphene layer. The epoxy complex undergoes transformation into a cyclic ether complex during the dioxiranyl decomposition. Transition states and energetic profiles of these decomposition reactions were determined. Variations of selected C−C, O−O, and C−O bonds were analyzed through the change in the bond orders calculated by natural bond orbital analysis. Overall, carbon oxidation reactions in the presence of epoxy functionalities are very important in the formation of heterogeneous CO_2 and of cyclic ether complexes.

1. Introduction

Combustion is the most widely used coal utilization process. Recently, however, gasification processes have received more attention due to their advantages over classic combustion technology, such as higher efficiency, higher variety of products (electricity, steam, syngas, and hydrogen), as well as better control of contaminant gases (SO_x, No_x, and CO_2). Gasification is carried out with an oxidant gas such as O_2, H_2O, or CO_2. In both combustion and gasification, two general steps can be distinguished in the processes: first, an oxygen atom is transferred from the oxidant molecule to the carbonaceous solid causing the formation of surface complexes, C(O); then these complexes can decompose giving rise to the formation of CO and/or CO_2 with the consequent consumption of the carbonaceous material.[1,2] It is important to mention that in coal combustion and gasification processes, CO_2 production is not only caused by surface complexes decomposition. In such processes, several secondary reactions can take place giving rise to CO_2 formation by homogeneous reactions in gaseous phase or other types of heterogeneous reactions such as CO readsorption on previously formed complexes.[3]

In the case of the oxidation with molecular oxygen, the first step is the dissociative chemisorption on the carbonaceous surface forming C(O) complexes that act as stable intermediates during the total process.[4] The general description of the process is shown by simple representations such as $O_2 + C_f \rightarrow 2C(O)$, where C_f represents an active site.[1,5] However, this description does not offer sufficient information at a molecular level of the elemental reactions taking place. In order to get an insight into the reactions that produce CO or CO_2, it is important to have the characterization of the complexes formed in the initial steps and their transformation during the process. To determine the nature of these complexes several experimental studies have been carried out employing techniques such as IR, NMR, X-ray photoelectron spectroscopy (XPS), scanning electron microscopy, transmission electron microscopy, temperature programmed desorption (TPD), and transient kinetics (TK),[3,6−18] among others.

One of the most common techniques in complexes characterization is TPD since it allows suggesting the nature of functional groups through their decomposition products. For example, the carboxilate groups generally decompose as CO_2, while ether, phenol, or carbonyl functionalities decompose as CO.[19] However, interpretation of the TPD profiles presents additional difficulties due to several secondary reactions.[3,7] B. Marchon et al.[20] used TPD to calculate desorption activation energies of CO and CO_2 and compared the determined values with those reported for bond energies of lactones, carbonyls, and semiquinones on reference compounds. A good correlation was obtained suggesting the presence of these functionalities on the carbonaceous materials during combustion or gasification processes. TPD may be used simultaneously with other techniques to obtain more detailed information of the functional groups giving rise to the CO or CO_2 thus formed. Kelemen and Freund[12] employed TPD and XPS to evaluate the decrease of the XPS signal of different complexes correlating them with the desorbed gases. This procedure allowed the researchers to observe that during CO_2 desorption the 288.8 eV C(1s) XPS signal diminishes. This signal corresponds to carbon atoms bonded to oxygen atoms by means of three bonds, suggesting the presence of carboxilate or carbonate groups that decompose as CO_2. These authors also found that the signal corresponding to C−O single bond (285.8 eV C(1s)), is the only signal remaining in XPS at high temperatures while CO evolution continues, allowing them to suggest the existence of an ether-

* Corresponding author. E-mail: fmondra@catios.udea.edu.co.

10.1021/jp065701i CCC: $37.00
Published on Web 12/09/2006

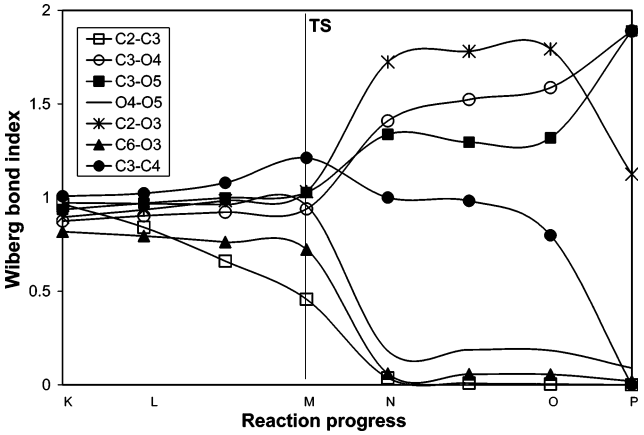

Figure 8. Formation and breaking of bonds on C(2O) decomposition to form CO_2(g) and ether-like complex. Letters K−P correspond to the structures in Figure 7.

functionality, the activation energy required for the CO_2 evolution would be very high and other reactions, such as O−O cleavage, may become more favorable.

The above-described step sequence can also be analyzed following the variation of the Wiberg bond index through the reaction coordinate. The changes are shown in Figure 8 where the NBO data of the main bonds involved in the decomposition of the oxidized graphene layer are plotted in the same figure. It is important to observe that in general the changes before the transition state are moderated. However, when the energy barrier is surpassed, some of the bonds undergo drastic reorganization. For example, the bond index of the C_2-O_3 bond of the epoxy group is near 1.0 until the transition state, then it acquires an index of about 1.8 indicating that the bond is very close to that of a double bond in the carbonyl group, and then again it becomes close to 1.0 when it forms the ether bond. In the case of the C_3-C_4 bond, the transition is more gradual as seen in Figure 8 while other bonds are almost completely cleaved after the transition state (C_6-O_3, C_2-C_3). This type of figure illustrates very clearly the bond transformations that take place in a chemical reaction.

In the research carried out by Haydar et al.[14] to evaluate desorption steps of CO_2, they found two CO_2 desorptions with activation energies at around 48 and 61 kcal/mol which were presented without assignation to any particular complex. In the present work, we reported two complexes which have CO_2 desorption activation energies similar to those found experimentally that may explain such desorptions.

Cyclic ether complexes have been reported in numerous studies by means of spectroscopic techniques.[6,12,15] However, to the best of our knowledge their formation mechanisms have not yet been described. In this study, we show a possible route for formation of such a complex that at the same time allows us to explain CO and CO_2 desorption in carbon gasification at high temperatures.

Finally, it is crucial to point out that the role of the epoxy group is different when it is located in the center of a graphene layer. In this case, the C−C bonds at the basal plane are broken and new ether bonds (C−O−C) are formed releasing the strain involved in the three-member ring structure as observed by Li et al.[22] The ether functionalities thus formed cause a deformation of the graphene layer that can explain the wrinkled and rough structure of an exfoliated graphite oxide observed by AFM.[25] Furthermore these complexes are also involved in the CO_2 desorption giving rise to vacancies in the interior of a graphene sheet.[25]

4. Conclusions

A step by step analysis of the oxidation of a graphene layer was carried out. This study suggests two possible routes for heterogeneous CO_2 desorption in oxidation with molecular oxygen of carbon materials. The first one takes place by means of a secondary reaction giving rise to the formation of a carbonate group at the edge of the graphene layer which decomposes as CO_2 leaving an isolated active site. The second reaction occurs through molecular chemisorption of O_2 on a graphene layer which has undergone a certain degree of oxidation, and therefore, there are other oxygenated complexes such as semiquinone and epoxy groups. Following these conditions, a mechanism for heterogeneous evolution of CO_2 and simultaneous formation of cyclic ether is proposed. This mechanism is useful to explain different experimental observations concerning CO_2 and CO desorption at high temperatures. At the same time, it explains the role of epoxy groups as oxygen reservoir in combustion and gasification reactions. Finally, the analysis of the bond order by NBO facilitates the understanding of the formation, transformation and cleavage of bonds involved in a given reaction, particularly when it is presented graphically as has been done in this research.

Acknowledgment. The authors thank the University of Antioquia for the financial support of the Young Researcher Program, the *Sostenibilidad* Program. We also thank Colciencias, Isagen, and University of Antioquia for the financial support of project 1118-06-17573. A.S. thanks Colciencias and the University of Antioquia for her Ph.D. scholarship.

References and Notes

(1) Moulijn, J. A.; Kapteijn, F. *Carbon* **1995**, *33*, 1155.
(2) Frankcombe, T.; Bhatia, S.; Smith, S. *Carbon* **2002**, *40*, 2341.
(3) Hall, P. J.; Calo, J. M. *Energy Fuels* **1989**, *3*, 370.
(4) Nozaki, T.; Adschiri, T.; Fujimoto, K. *Energy Fuels* **1991**, *5*, 610.
(5) Chen, N.; Yang, R. *J. Phys. Chem. A* **1998**, *102*, 6348.
(6) Zhuang, Q.-L.; Kyotani, T.; Tomita, A. *Energy Fuels* **1994**, *8*, 714.
(7) Zhuang, Q.; Kyotani, T.; Tomita, A. *Energy Fuels* **1995**, *9*, 630.
(8) Wong, C.; Yang, R. T.; Halpern, B. L. *J. Chem. Phys.* **1983**, *78*, 3325.
(9) Radovic, L. R.; Jiang, H.; Lizzio, A. A. *Energy Fuels* **1991**, *5*, 68.
(10) Mawhinney, D.; Yates, J. *Carbon* **2001**, *39*, 1167.
(11) Lynch, B. M.; Lancaster, L. I.; MacPhee, J. A. *Energy Fuels* **1988**, *2*, 13.
(12) Kelemen, S. R.; Freund, H. *Energy Fuels* **1988**, *2*, 111.
(13) He, H.; Riedl, T.; Lerf, A.; Klinowski, J. *J. Phys. Chem.* **1996**, *100*, 19954.
(14) Haydar, S.; Moreno-Castilla, C.; Ferro-García, M.; Carrasco-Marín, F.; Rivera-Utrilla, J.; Perrard, A.; Joly, J. *Carbon* **2000**, *38*, 1297.
(15) Fanning, P. E.; Vannice, M. A. *Carbon* **1993**, *31*, 721.
(16) Gozzi, D.; Guzzardi, G.; Salleo, A. *Solid State Ionics* **1996**, *83*, 177.
(17) Grzybek, T.; Kreiner, K. *Langmuir* **1997**, *13*, 909.
(18) Hontoria-Lucas, C.; López-Peinado, A. J.; López-González, J. d. D.; Rojas-Cervantes, M. L.; Martín-Aranda, R. M. *Carbon* **1995**, *33*, 1585.
(19) Boehm, H. *Carbon* **2002**, *40*, 145.
(20) Marchon, B.; Tysoe, W. T.; Carraza, J.; Heinemann, H.; Somorjai, G. A. *J. Phys. Chem.* **1988**, *92*, 5744.
(21) Pan, Z.; Yang, R. T. *Ind. Eng. Chem. Res.* **1992**, *31*, 2675.
(22) Li, J.-L.; Kudin, K. N.; McAllister, M. J.; Prud'homme, R. K.; Aksay, I. A.; Car, R. *Phys. Rev. Lett.* **2006**, *96*, 176101(1−4).
(23) Ajayan, P. M.; Yakobson, B. I. *Nature* **2006**, *441*, 818.
(24) Paredes, J.; Martínez-Alonso, A.; Tascón, J. *Carbon* **2000**, *38*, 1183.
(25) Schniepp, H. C.; Li, J.-L.; McAllister, M. J.; Sai, H.; Herrera-Alonso, M.; Adamson, D. H.; Prud'homme, R. K.; Car, R.; Saville, D. A.; Aksay, I. A. *J. Phys. Chem. B* **2006**, *110*, 8535.
(26) Incze, A.; Pasturel, A.; Chatillon, C. *Appl. Surf. Sci.* **2001**, *177*, 226.
(27) Incze, A.; Pasturel, A.; Peyla, P. *Phys. Rev. B* **2004**, *70*, 212103.
(28) Chen, N.; Yang, R. *Carbon* **1998**, *36*, 1061.
(29) Chen, S. G.; Yang, R. T.; Kapteijn, F.; Moulijn, J. A. *Ind. Eng. Chem. Res.* **1993**, *32*, 2835.

Available online at www.sciencedirect.com
ScienceDirect
Journal of the Mechanics and Physics of Solids
54 (2006) 2304–2329

JOURNAL OF THE MECHANICS AND PHYSICS OF SOLIDS

www.elsevier.com/locate/jmps

An atomistic and non-classical continuum field theoretic perspective of elastic interactions between defects (force dipoles) of various symmetries and application to graphene

X. Zhang[a], K. Jiao[c], P. Sharma[a,b,*], B.I. Yakobson[c,d]

[a]*Department of Mechanical Engineering, University of Houston, Houston, TX 77204, USA*
[b]*Department of Physics, University of Houston, Houston, TX 77204, USA*
[c]*Department of Mechanical Engineering and Materials Science, Rice University, Houston, TX 77204, USA*
[d]*Department of Chemistry, Rice University, Houston, TX 77204, USA*

Received 13 March 2006; received in revised form 24 June 2006; accepted 30 June 2006

Abstract

Force multipoles are employed to represent various types of defects and physical phenomena in solids: point defects (interstitials, vacancies), surface steps and islands, proteins on biological membranes, inclusions, extended defects, and biological cell interactions among others. In the present work, we (i) as a prototype simple test case, conduct quantum mechanical calculations for mechanics of defects in graphene sheet and in parallel, (ii) formulate an enriched continuum elasticity theory of force dipoles of various anisotropies incorporating up to second gradients of strain fields (thus accounting for nonlocal dispersive effects) instead of the usual dispersion-less classical elasticity formulation that depends on just the strain (c.f. Peyla, P., Misbah, C., 2003. Elastic interaction between defects in thin and 2-D films. Eur. Phys. J. B. 33, 233–247). The fundamental Green's function is derived for the governing equations of second gradient elasticity and the elastic self and interaction energies between force dipoles are formulated for both the two-dimensional thin film and the three-dimensional case. While our continuum results asymptotically yield the same interaction energy law as Peyla and Misbah for large defect separations ($\sim 1/r^n$ for defects with n-fold symmetry), the near-field interactions are qualitatively far more complex and free of singularities. Certain qualitative behavior of defect mechanics predicted by atomistic calculations are well captured by our

*Corresponding author. Department of Mechanical Engineering, Department of Physics, University of Houston, Houston, TX 77204, USA. Tel.: +1 713 743 4256.
E-mail address: psharma@uh.edu (P. Sharma).

0022-5096/$ - see front matter
doi:10.1016/j.jmps.2006.06.007

Gairola, B., 1976. Nonlocal theory of elastic interaction between point defects. Archi. Mech.
Garikipati, K., Falk, M., Bouville, M., Puchala, B., Narayanan, H., 2006. The continuum elastic and atomistic viewpoints on the formation volume and strain energy of a point defect. J Mech. Phys. Solids. 54 (9), 1929–1951.
Ghim, C., Park, J., 2002. Oriental dependence of fluctuation-induced interactions in biological membranes. J. Korean Phys. Soc. 40 (6), 1077–1081.
Gutkin, M., 2000. Nanoscopics of dislocation and disclinations in gradient elasticity. Rev. Adv. Mater. Sci. 1, 27–60.
Gutkin, M., Aifantis, E.C., 1999a. Dislocations in gradient elasticity. Scr. Mater. 40 (5), 559.
Gutkin, M., Aifantis, E.C., 1999b. Dislocations and disclinations in the gradient elasticity. Fiz. Tverdogo 41 (12), 2158.
Hirth, J., Lothe, J., 1982. Theory of Dislocations. Wiley, New York.
Jiang, H., Feng, X.Q., Huang, Y., Hwang, K.C., Wu, P.D., 2004. Defect nucleation in carbon nanotubes under tension and torsion: Stone–Wales transformation. Comput. Methods Appl. Mech. Eng. 193, 3419–3429.
Kleinert, H., 1989. Gauge Fields in Condensed Matter, World Scientific, Singapore.
Koiter, W., 2005. Couple stresses in the theory of elasticity, I and II. Proc. K. Ned. Akad. Wet. (B) 67, 17–44.
Kukta, R., Peralta, A., Kouris, D., 2002a. Elastic interaction of surface steps: effect of atomic-scale roughness. Phys. Rev. Lett. 88 (18), 186102-1–186102-4.
Kukta, R., Peralta, A., Kouris, D., 2002b. Surface steps: from atomistic to continuum. J. Appl. Mech., Trans. ASME 69 (4), 443–450.
Lazar, M., Maugin, G., Aifantis, E., 2005. On dislocations in a special class of generalized elasticity. Phys. Stat. Sol. B 242 (12), 2365–2390.
Lazar, M., Maugin, G., Aifantis, E., 2006. Dislocations in second strain gradient elasticity. Int. J. Solids Struct. 44, 1787.
Li, J.-L., Kudin, K.N., McAllister, M.J., Prud'homme, R.K., Aksay, I.A., Car, R., 2006. Oxygen-driven unzipping of graphitic materials. Phys. Rev. Lett. 96, 176101.
Li, Z., Dharap, P., Sharma, P., Nagarajaiah, S., Yakobson, B., 2005. Continuum field model of defect formation in carbon nanotube. J. Appl. Phys. 97, 074303.
Liu, B., Jiang, H., Huang, Y., Qu, S., Yu, M.-F., Hwang, K.C., 2005. Atomic scale finite element method in multiscale computation with applications to carbon nanotubes. Phys. Rev. B 72 (3), 35435.
Love, A., 1944. A Treatise on the Mathematical Theory of Elasticity, 4th ed. New York, Dover.
Marchenko, V., Misbah, C., 2005. Elastic interaction of point defects on biological membranes. Eur. Phys. J. E 8, 477–484.
Mindlin, R., 1965. Second gradient of strain and surface-tension in linear elasticity. Int. J. Solids Struct. 1, 417–438.
Mura, T., 1987. Micromechanics of Defects in Solids. Martinus Nijhoff, Hague, The Netherlands.
Nardelli, M.B., Yakobson, B.I., Bernholc, J., 1998. Mechanism of strain release in carbon nanotubes. Phys. Rev. B 57 (8), 4277.
Peyla, P., Misbah, C., 2003. Elastic interaction between defects in thin and 2D films. Eur. Phys. J. B 33, 233–247.
Reid, A., Gooding, R., 1992. Inclusion problem in a two-dimensional nonlocal elastic solid. Phys. Rev. B 46, 6045.
Ronda, A., Berbezier, I., 2004. Self-patterned Si surfaces as templates for Ge islands ordering. Physica E 23, 370.
Samsonidze, G., Samsonidze, G., Yakobson, B., 2002. Energetics of Stone–Wales defects in deformations of monoatomic hexagonal layers. Comput. Mater. Sci. 23, 62–72.
Schwarz, U., Balaban, N., Riveline, D., Bershadsky, A., Geiger, B., Safran, S., 2002. Calculation of forces at focal adhesions from elastic substrate data: the effect of localized force and the need for regularization. Biophys. J. 83, 1380–1394.
Shibutani, Y., 1998. Nonlocal elastic constants of centrosymmetric homogeneous lattice structure and inhomogeneous one. JSME Int. J., Ser. A (Solid Mech. Mater. Eng.) 41 (4), 547–553.
Shibutani, Y., Vitek, V., Bassani, J., 1998. Nonlocal properties of inhomogeneous structures by linking approach of generalized continuum to atomistic model. Int. J. Mech. Sci. 40 (2–3), 129–137.
Schwarz, U., Safran, S., 2002. Elastic interactions of cells. Phys. Rev. Lett. 88, 245416–245418.
Siems, R., 1968. Mechanical interactions of point defects. Phys. Stat. Sol. 30, 645.
Stewart, J.P.J., 1989. Optimization of parameters for semiempirical methods I. Method. J. Comput. Chem. 10, 209.

T. NÜCHTER

ANIMAL BIOLOGY

Good shot

Curr. Biol. **16,** R316–R318 (2006)

Jellyfish stings can puncture their targets with the power of rifle bullets, say researchers in Germany. The study reveals intriguing insight into how these tiny structures, known as cnidae, penetrate the tough skins of prey.

Thomas Holstein of the University of Heidelberg and his colleagues used an ultra-high-speed ballistics camera to watch stinging cells from the jellyfish-like animal *Hydra* (pictured right) discharge. They calculated that the sharply pointed stings were released at speeds of up to 40 metres per second (140 kph), with an acceleration of 5.4×10^6 *g*, resulting in a pressure on impact of 7 gigapascals.

This movement, one of nature's fastest, owes its force to powerful spring-like proteins that contract when the pressure in the cnidae drops as they discharge.

NEUROBIOLOGY

Same but different

Neuron **50,** 589–601; 603–616 (2006)

GABA (γ-aminobutyric acid), the main inhibitory chemical in the vertebrate nervous system, has many different modes of action. This is partly thanks to the precise location and activity of one of its receptor components, two new studies reveal.

The $GABA_B$ receptor is made of two pieces, and one piece known as $GABA_{B1}$ comes in two versions: $GABA_{B1a}$ and $GABA_{B1b}$. Teams in Switzerland led by Bernhard Bettler of the University of Basel and Matthew Larkum of the University of Bern studied mice in which the different $GABA_{B1}$ versions were inactivated one at a time.

They found that $GABA_{B1a}$ localizes to one side of the neuronal synapse and helps to inhibit the release of neurotransmitters, whereas $GABA_{B1b}$ localizes to the opposite side, where it helps to dampen neuronal firing of post-synaptic cells.

MICROBIOLOGY

Stripped bare

PLoS Pathogens **2,** e35 (2006)

Researchers in the United States have uncovered a network of genes that shields a fungus' cell wall from immune-system attack.

In disease-causing fungi, an outer coat protects an inner layer of a sugary protein called β-glucan. Robert Wheeler and Gerald Fink of the Whitehead Institute for Biomedical Research in Cambridge, Massachusetts, screened a library of 4,800 mutant yeast strains to find genes that, when disabled, expose the β-glucan. They showed that disabling nearly 50 of these genes makes fungi more vulnerable to attack by mouse immune cells.

Targeting the proteins made by the masking genes might yield much-needed medicines to fight insidious pathogenic fungi such as *Candida albicans*.

MATERIALS

Graphite unzipped

Phys. Rev. Lett. **96,** 176101 (2006)

Graphene — a single graphite-like carbon sheet — has unusual and potentially useful electronic behaviour. But it is hard to make. One promising approach involves oxidizing graphite to form graphite oxide, which separates layer by layer into thin flakes.

These flakes are generally much smaller than the original layers, and now Je-Luen Li and colleagues at Princeton University, New Jersey, think they know why.

The team identified bright lines in microscopic images of graphite oxide as fault lines where the layers have cracked. Their quantum-chemical calculations showed that these cracks are created by an 'unzipping' process in which the cooperative bonding of oxygen atoms next to one another on the surface creates a row of broken carbon–carbon bonds.

CHEMISTRY

Clean sweep

Science **312,** 1024–1026 (2006)

Hydrogen atoms can now be stripped from a silicon surface using laser light in a process that generates virtually no heat. Hydrogen desorption is an important part of computer-chip manufacture that normally requires temperatures of around 800 °C, which can introduce defects into the chips.

The technique, developed by Philip Cohen from the University of Minnesota, Minneapolis, and his colleagues, is highly selective, picking off hydrogen but leaving atoms of its heavier isotope deuterium behind. This shows that there is no transfer of heat across the silicon surface, as this would cause both hydrogen isotopes to desorb.

JOURNAL CLUB

Catherine L. Drennan
Massachusetts Institute of Technology, USA

A biochemist considers cool inorganic chemistry that is relevant to our energy crisis.

There is a class of enzymes, found in certain microorganisms, that are the envy of synthetic chemists. They catalyse the reversible conversion of carbon dioxide (CO_2) to carbon monoxide (CO) — a difficult feat in the lab because the carbon–oxygen double bond in CO_2 is very strong.

In striving to match nature's success, chemists seek twofold environmental benefits: making CO — a useful feedstock for synthesizing carbon compounds — without using precious fossil fuels while, at the same time, consuming the greenhouse gas CO_2.

After my group solved the crystal structure for two of these enzymes, known as carbon monoxide dehydrogenase/acetyl-CoA synthase, I sought out the company of Joseph Sadighi, an assistant professor in my department, to discuss possible mechanisms involving the use of the enzymes' nickel–iron–sulphur clusters as catalysts. Sadighi was searching for other first-row transition metals that could catalyse the same reaction.

As my research took me in new directions, our long conversations about CO_2 came to an end. I heard occasional updates on his progress, but it wasn't until last October that I learnt the full story. I received a preprint of a paper from Sadighi and his co-workers announcing their new catalyst for CO_2 reduction (D. S. Laitar, P. Müller & J. P. Sadighi *J. Am. Chem. Soc.* **127,** 17196–17197; 2005). Instead of nature's choice of iron and nickel, they had prepared copper(I) boryl complexes. These catalysts convert an impressive 100 molecules of CO_2 per hour at room temperature.

This is not only an exciting development in catalysis, it also shows the potential of inorganic chemistry in tackling our environmental problems.

Computational Studies of the Structure, Behavior upon Heating, and Mechanical Properties of Graphite Oxide

Jeffrey T. Paci,*,† Ted Belytschko,‡ and George C. Schatz*,†

Department of Chemistry, Northwestern University, 2145 Sheridan Road, Evanston, Illinois 60208-3113, and Department of Mechanical Engineering, Northwestern University, 2145 Sheridan Road, Evanston, Illinois 60208-3111

Received: July 23, 2007; In Final Form: September 14, 2007

A Monte Carlo based scheme for the formation of graphite oxide (GO) was developed and implemented. A Rosenbluth factor was used to select intermediate structures in an attempt to form stable, low-energy, and realistic GO. The scheme resulted in the production of GO that has an interplanar spacing of 5.8 Å, in good agreement with the experimental value (5.97 Å). Epoxide and hydroxyl functional groups dominate the basal planes, a finding that is consistent with experiment. Individual sheets are wrinkled with an average root-mean-square deviation of 0.33 ± 0.04 Å. Hydrogen bonding between hydroxyl groups and between hydroxyl and epoxide groups has significant impact on the stability of many structures. Molecular dynamics simulations, guided by forces from electronic structure calculations, were performed to examine the behavior of GO when heated to room (300 K) and thermal exfoliation (1323 K) temperatures. Hydrogen-transfer reactions that catalyze the migration of epoxide groups were observed at both temperatures. At 1323 K, the evolution of CO was also observed, and the mechanisms for this process have been elucidated. This process provides a plausible explanation of the source of the 30% carbon mass loss that occurs during the experimental thermal exfoliation of GO. The mechanical properties of GO were examined and compared to those of graphene. Although significantly weaker in tensile deformation than graphene (fracture stress = 116 GPa), GO (fracture stress = 63 GPa) potentially has great strength provided it does not contain large holes. An epoxide line defect, recently reported as playing an important role in the failure of oxidized graphene, was also examined. The observed very large fracture stress (97 GPa) suggests that this structure does not play a major role in the fracture process.

I. Introduction

Interest in graphite oxide (GO) has increased recently because of its potential as a starting material for the large-scale production of exfoliated two-dimensional graphite nanosized platelets, which have shown considerable promise as a nanocomposite filler material.[1−4] Graphite oxide was first synthesized in 1859 by treating graphite (an inexpensive starting material) with $KMnO_4$ and H_2SO_4[5] and has since been synthesized using a variety of oxidative methods.[6,7] In most cases, the planar structure of graphite is preserved, with the interplanar spacing increasing from 3.4 Å (the interplanar spacing in graphite) to a value of at least 6.0 Å. This spacing increases with oxidant/acid exposure time and subsequent exposure to moisture. Although the oxidation process can be continued until CO and CO_2 are eventually produced from the parent graphite, well-structured GOs have been reported with oxygen levels in approximate stoichiometries as high as $C_{10}O_5H_2$.[8]

Graphite oxide readily forms stable colloidal dispersions of thin sheets in water.[9−11] It can be hydrophobized using *n*-alkylammonium cations and swollen in organic solvents, resulting in lamellar GO structures whose size can be controlled by adjusting solvent composition.[12] Treating GO with organic isocyanates[13] creates a material that readily forms stable dispersions in polar aprotic solvents and that spontaneously exfoliates into individual graphite oxide sheets with a thickness of ∼1 nm.[3] These sheets mix readily with many organic polymers, making possible the synthesis of graphene−polymer composites.[3] Chemical reduction of composites containing GO can result in materials that are electrically conductive[1,3,14,15] due to regraphitization. Several GO-containing composites have been shown to possess properties that make them suitable for use as cathodic materials in lithium rechargeable batteries (see, e.g., refs 2 and 16).

Rapid heating also can be used to exfoliate GO into single sheets. A heating rate greater than 2000 °C/min for 30 s in a 1323 K oven has been used to create well-dispersed sheets that exhibit a lateral extent of a few hundred nanometers.[17] A mass loss of 30% accompanies this exfoliation and suggests that the sheets may contain a significant number of defects and that these defects could be of a significant size.

The graphene sheets in GOs are decorated with a variety of functional groups. There is extensive NMR, infrared spectroscopic, and electron diffraction evidence for the presence of COOH, OH, and C=O groups at the edges of the sheets while the basal planes are covered with mostly epoxide (1,2-ether) and OH functionalities.[8,18−24] A large number and variety of models of this material have been proposed.[8,10,18−21,25−30] Although there also has been some preliminary theoretical work performed in an attempt to understand this material,[17,31] much remains to be learned about its structural details.

* Author to whom correspondence should be addressed. E-mail: jpaci@chem.northwestern.edu; schatz@chem.northwestern.edu.
† Department of Chemistry.
‡ Department of Mechanical Engineering.

10.1021/jp075799g CCC: $37.00
Published on Web 11/08/2007

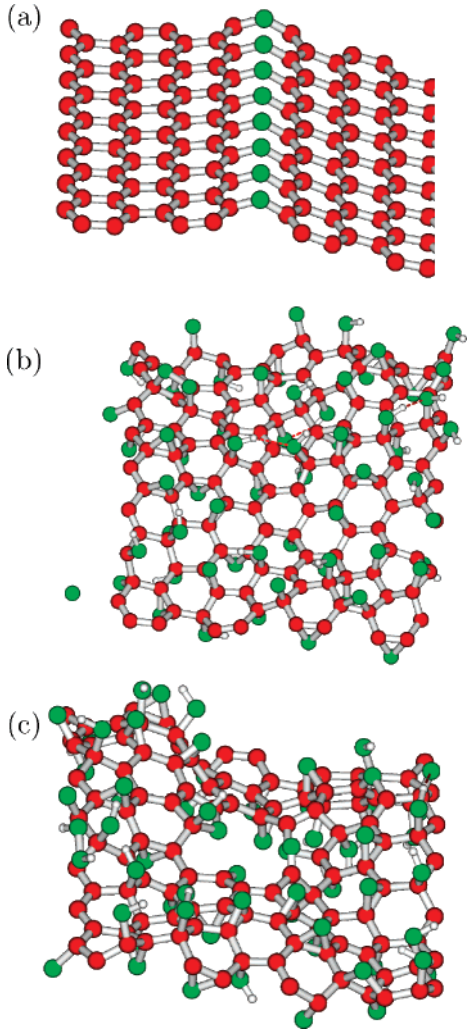

Figure 9. (a) Graphene sheet containing an epoxide line defect, (b) the pristine GO sheet, and (c) the GO sheet that was initially missing a hexagonal unit of carbon atoms that were strained to failure. Their stress versus strain behavior is shown in Figure 8.

This is important because structures that are relatively low in energy at low oxidation levels do not necessarily lead to relatively low-energy structures at higher oxidation levels. The process was repeated in stages in which additional functional groups were added to the sheets, until an experimentally observed stoichiometry was synthesized. Sheets containing various defects were also examined.

The resulting GO sheets were significantly wrinkled. The calculated interplanar spacing of 5.8 Å for the pristine sheets is in good agreement with observed experimental values (5.97 Å). A complex set of hydroxyl−hydroxyl and hydroxyl−epoxide hydrogen-bonding interactions takes place between the functional groups. Occasionally, small holes in the basal planes appear as C−C bonds break. The resulting potentially dangling bond carbons form carbonyl and alcohol groups. Other molecules, such as peroxide and water molecules, are also observed.

Molecular dynamics simulations were performed to examine the behavior of GO upon heating to room (300 K) and thermal-exfoliation (1323 K) temperatures. These MD simulations used forces obtained from SCC-DFTB electronic structure calculations. At both temperatures, reactions in which hydrogen atoms are transferred were observed. Also, epoxide groups were observed to migrate on the basal plane in processes often stabilized by hydrogen bonding or catalyzed by hydrogen-transfer reactions between the mobile epoxide oxygen and neighboring functional groups. At 1323 K, CO evolution from pristine sheets and those containing pre-existing defects was observed. This CO evolution provides a plausible explanation for the 30% carbon mass loss that occurs during the thermal exfoliation of GO.

The mechanical properties of GO were examined and were compared to those of graphene. Oxidation was found to decrease the strength by 46%. A nanohole formed by removing a single cluster of carbon atoms in a 128 atom sheet was found to reduce the strength by more than 63%, so the effects of nanodefects may be significantly more deleterious on strength than oxidation. The reduction in fracture stress due to epoxide line defects was found to be less than 17% as compared to a pristine sheet, which indicates that these have little effect on the strength.

Acknowledgment. We gratefully acknowledge grant support from the National Science Foundation (Grant No. CMS 500304472), the NASA University Research, Engineering, and Technology Institute on Bio-Inspired Materials under Award No. NCC-1-02037, and the Air Force Office of Scientific Research (Grant No. FA955D-07-1-0095). J.T.P. thanks A. Lerf for helpful correspondence during the early stages of this work.

References and Notes

(1) Szabó, T.; Szeri, A.; Dékány, I. *Carbon* **2005**, *43*, 87.
(2) Du, X. S.; Xiao, M.; Meng, Y. Z.; Hay, A. S. *Carbon* **2005**, *43*, 195.
(3) Stankovich, S.; Dikin, D. A.; Dommett, G. H. B.; Kohlhaas, K. M.; Zimney, E. J.; Stach, E. A.; Piner, R. D.; Nguyen, S. T.; Ruoff, R. S. *Nature* **2006**, *442*, 282.
(4) Cerezo, F. T.; Preston, C. M. L.; Shanks, R. A. *Macromol. Mater. Eng.* **2007**, *292*, 155.
(5) Brodie, B. C. *Philos. Trans. R. Soc. London* **1859**, *149*, 249.
(6) Staudenmaier, L. *Ber. Dtsch. Chem. Ges.* **1898**, *31*, 1481.
(7) Hummers, W. S., Jr.; Offeman, R. E. *J. Am. Chem. Soc.* **1958**, *80*, 1339.
(8) Szabó, T.; Berkesi, O.; Forgó, P.; Josepovits, K.; Sanakis, Y.; Petridis, D.; Dékány, I. *Chem. Mater.* **2006**, *18*, 2740.
(9) Hofmann, U.; Frenzel, A. *Ber. Dtsch. Chem. Ges.* **1930**, *63*, 1248.
(10) Ruess, G. *Monatsh. Chem.* **1946**, *76*, 381.
(11) Stankovich, S.; Piner, R. D.; Chen, X.; Wu, N.; Nguyen, S. T.; Ruoff, R. S. *J. Mater. Chem.* **2006**, *16*, 155.
(12) Dékány, I.; Krüger-Grasser, R.; Weiss, A. *Colloid Polym. Sci.* **1998**, *276*, 570.
(13) Stankovich, S.; Piner, R. D.; Nguyen, S. T.; Ruoff, R. S. *Carbon* **2006**, *44*, 3342.
(14) Kotov, N. A.; Dékány, I.; Fendler, J. H. *Adv. Mater.* **1996**, *8*, 637.
(15) Bourlinos, A. B.; Gournis, D.; Petridis, D.; Szabó, T.; Szeri, A.; Dékány, I. *Langmuir* **2003**, *19*, 6050.
(16) Matsuo, Y.; Higashika, S.; Kimura, K.; Miyamoto, Y.; Fukutsuka, T.; Sugie, Y. *J. Mater. Chem.* **2002**, *12*, 1592.
(17) Schniepp, H. C.; Li, J.-L.; McAllister, M. J.; Sai, H.; Herrera-Alonso, M.; Adamson, D. H.; Prud'homme, R. K.; Car, R.; Saville, D. A.; Aksay, I. A. *J. Phys. Chem. B* **2006**, *110*, 8535.
(18) He, H.; Riedl, T.; Lerf, A.; Klinowski, J. *J. Phys. Chem.* **1996**, *100*, 19954.
(19) Lerf, A.; He, H.; Riedl, T.; Forster, M.; Klinowski, J. *Solid State Ionics* **1997**, *101−103*, 857.
(20) He, H.; Klinowski, J.; Forster, M.; Lerf, A. *Chem. Phys. Lett.* **1998**, *287*, 53.
(21) Lerf, A.; He, H.; Forster, M.; Klinowski, J. *J. Phys. Chem. B* **1998**, *102*, 4477.
(22) Szabó, T.; Berkesi, O.; Dékány, I. *Carbon* **2005**, *43*, 3181.
(23) Szabó, T.; Tombácz, E.; Illés, E.; Dékány, I. *Carbon* **2006**, *44*, 537.
(24) Aragon de la Cruz, F.; Cowley, J. M. *Nature* **1962**, *196*, 468.
(25) Hofmann, U.; Holst, R. *Ber. Dtsch. Chem. Ges.* **1939**, *72*, 754.
(26) Clauss, A.; Plass, R.; Boehm, H.-P.; Hofmann, U. *Z. Anorg. Allg. Chem.* **1957**, *291*, 205.
(27) Scholz, W.; Boehm, H.-P. *Z. Anorg. Allg. Chem.* **1969**, *369*, 327.
(28) Mermoux, M.; Chabre, Y.; Rousseau, A. *Carbon* **1991**, *29*, 469.
(29) Nakajima, T.; Mabuchi, A.; Hagiwara, R. *Carbon* **1988**, *26*, 357.
(30) Nakajima, T.; Matsuo, Y. *Carbon* **1994**, *32*, 469.
(31) Li, J.-L.; Kudin, K. N.; McAllister, M. J.; Prud'homme, R. K.; Aksay, I. A.; Car, R. *Phys. Rev. Lett.* **2006**, *96*, 176101.